On the interaction of vortices with mixing layers

Marcos Vera[a)] and Amable Liñán
Departamento de Motopropulsión y Termofluidodinámica, E.T.S.I. Aeronáuticos,
Universidad Politécnica de Madrid, 28040 Madrid, Spain

We describe the perturbations introduced by two counter-rotating vortices—in a two-dimensional configuration—or by a vortex ring—in an axisymmetric configuration—to the mixing layer between two counterflowing gaseous fuel and air streams of the same density. The analysis is confined to the near stagnation point region, where the strain rate of the unperturbed velocity field, A_0, is uniform. We restrict our attention to cases where the typical distance $2r_0$ between the vortices—or the characteristic vortex ring radius r_0—is large compared to both the thickness, δ_v, of the vorticity core and the thickness, $\delta_m \sim (\nu/A_0)^{1/2}$, of the mixing layer. In addition, we consider that the ratio, Γ/ν, of the vortex circulation, Γ, to the kinematic viscosity, ν, is large compared to unity. Then, during the interaction time, A_0^{-1}, the viscous and diffusion effects are confined to the thin vorticity core and the thin mixing layer, which, when seen with the scale r_0, appears as a passive interface between the two counterflowing streams when they have the same density. In this case, the analysis provides a simple procedure to describe the displacement and distortion of the interface, as well as the time evolution of the strain rate imposed on the mixing layer, which are needed to calculate the inner structure of the reacting mixing layer as well as the conditions for diffusion flame extinction and edge-flame propagation along the mixing layer. Although in the reacting case variable density effects due to heat release play an important role inside the mixing layer, in this paper the analysis of the inner structure is carried out using the constant density model, which provides good qualitative understanding of the mixing layer response. © *2004 American Institute of Physics.*
[DOI: 10.1063/1.1718956]

I. INTRODUCTION

The interaction of vortices with mixing layers is of great importance for the understanding of fundamental combustion processes, such as turbulent combustion and combustion instability.[1,2]

Often, the characteristic scales associated with the combustion processes are smaller than the smallest scales of the turbulence.[3] Then, combustion occurs in the form of laminar flames embedded in thin mixing layers that are locally distorted and strained by vortices of different scales. This has led to the development of a variety of flamelet models. These models consider a turbulent flame to be formed by an ensemble of laminar flamelets, which may be extinguished if subject to a supercritical local strain.[4]

Most flamelet models assume that a turbulent diffusion flame behaves locally as a steady, strained, one-dimensional, laminar flame.[5,6] This is the base of the so-called laminar flamelet assumption. However, steady strain models ignore several features of turbulence-combustion interactions. In particular, the unsteady response of combustion and transport processes to the variations in the turbulent field—which may induce extinction and reignition processes—and the effect of curvature—which may alter the flame structure through transverse diffusion—are removed. These limitations, discussed in detail by Cuenot and Poinsot,[7] have led to the

development of flamelet models including transient effects[8] and, more recently, to the development of the so-called unsteady flamelet approach.[9]

Recent theoretical, numerical, and experimental analyses have tried to quantify unsteady and curvature effects studying the response of a one-dimensional laminar flame to variable strain rate[5,10–15] and the interaction of vortices with flames (see the recent review article by Renard *et al.*[2] and references therein).

Aspects of the interaction of single vortices with reacting mixing layers—or diffusion flames—have been studied analytically by Marble,[16] Karagozian and Marble,[17] Baum *et al.*,[18] Cetegen and Sirignano,[19] and Liñán.[20] Similar investigations were carried out by Peters and Williams,[21] who analyzed the roll-up of a premixed flame by a single vortex, and by Karagozian and Manda,[22] who studied the effect of a pair of counter-rotating vortices on a diffusion flame. These analyses aimed to describe the flame structure, the global enhancement of the chemical reaction due to the vortex roll-up, and the structure of the burned core.

The interaction of vortices with flames has also been studied in different configurations both numerically[23–25] and experimentally[26–28] by several authors. In particular, the head-on interaction of a vortex pair or vortex ring with a laminar flame is a very simple configuration that has received great attention in the last years.[29–37] This kind of interaction provides relevant information such as the time evolution of the flame front,[38] the flame structure, as well as

a)Electronic mail: vera@tupi.dmt.upm.es

information on extinction limits, pocket formation, effects of vortex size and strength, etc.

The aim of this work is to contribute to the understanding of the response of mixing layers (or diffusion flames) to the perturbations by vortices, analyzing the simple configuration of the head-on interaction of laminar vortex pairs—or vortex rings—with counterflow strained mixing layers. The analysis will be carried out, assuming constant density, for the cases of interest when the thicknesses δ_m of the mixing layer and δ_v of the vorticity core of the vortices are small compared to the characteristic core to core distance or vortex ring radius r_0.

In this case, three characteristic times arise in the problem, the baseline strain time, A_0^{-1}, the turnover time of the vortices, $t_T \sim r_0^2/\Gamma$, and the viscous time, $t_v \sim r_0^2/\nu$, where A_0 denotes the (baseline) strain rate experienced by the unperturbed mixing layer and Γ denotes the strength of the vortices. Then, if the vortices are to maintain their identities during the interaction, the viscous time must be large compared to the other two time scales, $t_v \gg A_0^{-1}$ and $t_v \gg t_T$, which leads naturally to the assumption that both Reynolds numbers, $A_0 r_0^2/\nu$ and Γ/ν, must be large compared to unity. Then, the ratio of the baseline strain time to the turnover time, $t_T/A_0^{-1} \sim \Gamma/r_0^2 A_0 \sim 1$, assumed to be of order unity, emerges here as the main parameter of the problem. In this case we are allowed to neglect the viscous effects to obtain a simple description of the flow field and the evolution of the vortices and of the distorted mixing layer. The results of this analysis will be used later to describe the internal structure of the mixing layer.

One aspect of special relevance in this kind of interaction is the distortion of the mixing layer by the vortices, which increases the flame surface area and enhances molecular mixing. Here we shall analyze the effects of this distortion on the distribution in the mixing layer of the so-called mixture fraction Z, a conserved scalar of unit concentration in the fuel stream and zero concentration in the air stream. In the Burke–Schumann limit of infinite reaction rates, the mixture fraction characterizes the diffusion flame structure when the mass and thermal diffusivities are assumed to be equal. In this case, the flame sheet is located at the surface where Z takes its stoichiometric value Z_s, and the rate of fuel consumption per unit flame surface is characterized by the value $|\nabla Z|_s$ of the mixture fraction gradient at the stoichiometric surface. See, for example, the books of Williams[1] and Peters.[3]

When the effective activation energy of the overall reaction is large, diffusion flame extinction occurs, with small changes from the Burke–Schumann flame structure, when the thickness of the reaction layer, δ_r, is still small compared with the effective thickness, $\delta_m \sim |\nabla Z|_s^{-1}$, of the mixing layer. In fact, the local extinction of the flame occurs when the instantaneous value $\chi_s = D_T |\nabla Z|_s^2$ of the scalar dissipation rate at the stoichiometric surface, which is the inverse of the characteristic diffusion time δ_m^2/D_T, grows to values of the order of the inverse of the residence time D_T/S_L^2 across the preheated zone of the stoichiometric premixed flame.[3,4] Here D_T is the thermal diffusivity of the mixture and S_L

denotes the propagation velocity of the stoichiometric premixed flame.

Under near-extinction conditions, the structure of the thin reaction layer, with characteristic response time δ_r^2/D_T small compared with $\delta_m^2/D_T \sim \chi_s^{-1}$, is quasi-steady and quasi-planar during the time of interaction of the vortex and the mixing layer. The critical value of χ_s for extinction can then be taken to be equal to the extinction value $\chi_{s,e}$ of a planar steady diffusion flame, which can be obtained experimentally or using numerical calculations based on a detailed kinetic scheme. Nevertheless, unsteady effects play a key role in determining the evolution of the outer mixing layer structure, and therefore of χ_s, which in turn determines the conditions for the local extinction of the flame. For this reason, our main concern in this paper will be the description of the time and spatial evolution of χ_s during the vortex mixing layer interaction.

During the flame vortex interaction, local extinction of the flame will occur as soon as the transient scalar dissipation rate imposed by the vortex, which is roughly $\chi_s \sim t_T^{-1} \sim \Gamma/r_0^2$, increases above a certain critical value. This can be achieved both by decreasing the vortex size, r_0, which, on the other hand, reduces the Reynolds number of the flow, or, alternatively, by increasing the strength of the vortex, Γ, which increases the Reynolds number of the flow. Then, the main advantage of considering vortices that are both "large and strong" is that one is able to decouple the diffusive processes that occur at the vortex core (diffusion of vorticity) from those that take place at the mixing layer (diffusion of species), and that it is possible to use boundary-layer analysis.

The analysis could also be used for the description of the dynamics of triple flames, or of flame-edges, that form after the local extinction of diffusion flames. The local extinction of the flame leads to the formation of extinguished holes (or annulus), where both reactants mix without reaction. These regions are separated from the diffusion flame by a flame-edge that can propagate in either direction—as an ignition or extinction front—depending on the local flow conditions. Thus, for values of the scalar dissipation rate smaller than a critical value, $\chi_s < \chi_{s,\text{crit}}$, they propagate along the stoichiometric surface towards the unburned mixture in the form of triple flames (ignition fronts), while for $\chi_{s,\text{crit}} < \chi_s < \chi_{s,e}$ they behave as extinction fronts that recede away from the unburned mixture.[39,40] The detailed analysis of the scalar dissipation rate along the flame surface is therefore of interest for the subsequent evolution of extinguished holes.[34]

The characteristic scales of the vortices and of the mixing layer are introduced in Sec. II, while the dynamics of the vortices and the flow field are described in Sec. III. The formulation of the inner structure of the mixing layer is given in Sec. IV and the numerical results are presented in Sec. V. The asymptotic description of the interaction in the limits of large and small effective vortex strength is outlined in Secs. VI and VII. Finally, some conclusions are presented in Sec. VIII.

II. CHARACTERISTIC SCALES IN THE INTERACTION OF VORTEX PAIRS/RINGS WITH MIXING LAYERS

A. Freely propagating vortex pairs/rings

In this section we discuss the characteristic scales for the dynamics of vortex pairs, of circulation Γ and core to core distance $2r_c$, and of vortex rings, of circulation Γ and radius r_c, with a core thickness of size $\delta_v \ll r_c$.

For vortex pairs the characteristic length is r_c, while the characteristic velocity is $V_I = \Gamma/4\pi r_c$. This is the velocity of displacement of the vortex pair when the Reynolds number $\mathrm{Re}_\Gamma = \Gamma/\nu$, which is roughly the ratio of the diffusion time r_c^2/ν to the turnover time r_c/V_I, is large compared with unity. Note that the propagation velocity V_I of a vortex pair does not depend on the size of the vorticity core, if this size δ_v is small compared with r_c.

These scales are also applicable for vortex rings, although the velocity of self-propagation depends on the ratio δ_v/r_c in the form

$$V_I = \frac{\Gamma}{4\pi r_c}\left(\log\frac{8r_c}{\delta_v} - \frac{1}{4}\right), \tag{1}$$

as obtained by Lord Kelvin[41] for a circular core of uniform vorticity.

As it is well known,[42] the streamlines in the reference frame moving with the vortex pair or ring demonstrate the existence of a bubble of fluid that is transported by the vortices, which becomes doughnut shaped for vortex rings for small values of δ_v/r_c, such that

$$\frac{V_I}{\Gamma/2r_c} = \frac{1}{2\pi}\left(\log\frac{8r_c}{\delta_v} - \frac{1}{4}\right) > 1. \tag{2}$$

If the fluid used in the generation of the vortices and transported by them differs from the surrounding fluid, it is bounded by a mixing layer with a thickness of order $(\nu/A_T)^{1/2}$, where $A_T = V_I/r_c \sim \Gamma/4\pi r_c^2$ is the characteristic value of the strain due to the vortices. Thus, if we want the vortices to maintain their identities $(\nu/A_T)^{1/2}$ must be small compared with r_c, which is the case if $\Gamma/4\pi\nu \gg 1$.

B. Vortex pairs/rings subject to strain

We shall now analyze the dynamics of the vortices when they move, under the conditions $\mathrm{Re}_\Gamma \sim \Gamma/4\pi\nu = V_I r_c/\nu \gg 1$ and $\delta_v/r_c \ll 1$, in the straining flow field associated with two counter-flowing irrotational streams of the same density, and with a strain rate A_0. Our aim is to analyze the perturbations of the mixing layer by the vortices in cases where the thickness of the unperturbed mixing layer, $\delta_{m0} = (D_T/A_0)^{1/2}$, is small compared with r_c.

The motion of the vortices results from the superposition of the velocity due to the strain and the self-induced velocity V_I. As a consequence, the core to core distance of the vortex pair, or the vortex ring radius, will grow with time at rates

$$\frac{dr_c}{dt} = A_0 r_c \quad \text{and} \quad \frac{dr_c}{dt} = \frac{A_0}{2}r_c, \tag{3}$$

respectively. Then, in order to characterize the size of the vortices, we shall use the value r_0 of r_c at the time of cross-

FIG. 1. Schematic representation of the distortion by vortices of a mixing layer in the stagnation region between two gaseous counterflowing streams of fuel and air coming from $z \to -\infty$ and $z \to \infty$, respectively. The different variables used in the description of the flow are clearly indicated.

ing of the vortices through the original plane of the mixing layer. Here we are interested in cases where the Reynolds number

$$\mathrm{Re}_0 = \frac{r_0^2 A_0}{\nu} = \frac{1}{\mathrm{Pr}}\left(\frac{r_0}{\delta_{m0}}\right)^2 \tag{4}$$

is large compared with unity. In addition, we shall assume that the Prandtl number $\mathrm{Pr} = \nu/D_T$ is of order unity, as typically occurs for gaseous mixtures.

The dynamics of the vortex pair or vortex ring will depend on the nondimensional circulation of the vortices, $\tilde{\Gamma}$, defined below in (8) and (22) for vortex pairs and vortex rings, respectively, which is the ratio of the characteristic self-induced strain due to the vortices, and the basic strain A_0 of the unperturbed flow. For small values of $\tilde{\Gamma}$ the basic strain will rapidly transport the vortices to the mixing layer and increase r_c exponentially with time.

For large values of $\tilde{\Gamma}$ the interaction between the vortices and the basic strain involves two main time scales, the characteristic strain time, A_0^{-1}, and the turnover time of the vortices, $4\pi r_0^2/\Gamma$, which is small, by a factor $\tilde{\Gamma}^{-1}$, compared to A_0^{-1} when $\tilde{\Gamma} \gg 1$.

III. VORTEX DYNAMICS AND DISTORTION OF THE MIXING LAYER

Under the assumptions stated above, in the following sections we shall analyze the perturbations introduced by two counter-rotating vortices—in a two-dimensional configuration—or by a vortex ring—in an axisymmetric configuration—on the mixing layer in the stagnation region between two gaseous counter-flowing streams of fuel and air, as shown schematically in Fig. 1. Without loss of generality, we consider that in the two-dimensional case the symmetry

plane of the vortex pair coincides with that of the basic strain, and in the axisymmetric case the vortex ring is coaxial with the basic flow.

When both streams have the same density, the unperturbed potential velocity field near the stagnation point is given by $v = -A_0 z$ and $u = A_0 r$ in the planar case, and by $v = -A_0 z$ and $u = A_0 r/2$ in the axisymmetric case. Here r and z denote the radial and axial Cartesian coordinates tangential and transverse to the unperturbed mixing layer, respectively, and u and v represent the corresponding velocity components along the r and z axes.

The perturbed mixing layer, whose thickness δ_m is infinitely thin compared with r_0 in the limiting case, $\Gamma/\nu \gg 1$ and $r_0^2 A_0/\nu \gg 1$, that we are analyzing, is seen as a passive interface between the two counter-flowing fluids when these have the same density. The variable density effects, due to the heat release in the mixing layer, will be dependent on the outer velocity and pressure fields generated by the dynamics of the vortices, which is independent of the internal dynamics of the mixing layer.

Effectively, due to thermal expansion, the mixing layer can be viewed as a planar distribution of volume sources that induces transversal displacement velocities. These velocities generate an irrotational perturbation flow that has to be added to the outer irrotational flow due to the baseline strain and the vortices. This perturbation flow could be able to modify the vortex path if the displacement velocities were strong enough. However, this is not the case in the limiting case considered here. Using order of magnitude estimates, it is easy to see that the ratio of the (viscous) transversal displacement velocities, $v_m \sim (\nu A_T)^{1/2} = (\nu V_I/r_c)^{1/2}$, to the characteristic velocity of the vortices, $V_I = \Gamma/4\pi r_c$, is of order

$$v_m/V_I \sim (\nu/V_I r_c)^{1/2} = (4\pi\nu/\Gamma)^{1/2}, \tag{5}$$

which is clearly small when the Reynolds number $\Gamma/4\pi\nu$ is large. Therefore, being consistent with the approximation of thin-cored vortices, which required the assumption $\Gamma/4\pi\nu \gg 1$, we may also neglect the effect of thermal expansion on the outer irrotational streams.

The interaction between the vortices and the mixing layer is much more complex in the more general case of counter-flowing streams with different densities,[43,44] which is not treated here. In this case vorticity is generated at the interface by baroclinic effects, which affects strongly the dynamics of the vortices and the interface distortion. This, in turn, modifies the local values of the strain rate, whose time evolution ultimately determines the flame response.

A. The two-dimensional case

The velocity field associated with the vortex pair, of circulation Γ and core position $r_c(t)$ and $z_c(t)$, has to be added to the unperturbed straining field to obtain the instantaneous velocity field, thus allowing us to calculate the time evolution of the vortex core position.

The evolution of r_c and z_c with time is obtained by evaluating u and v at the vortex core (r_c, z_c) leaving out the local self-induced velocity due to the vortex,
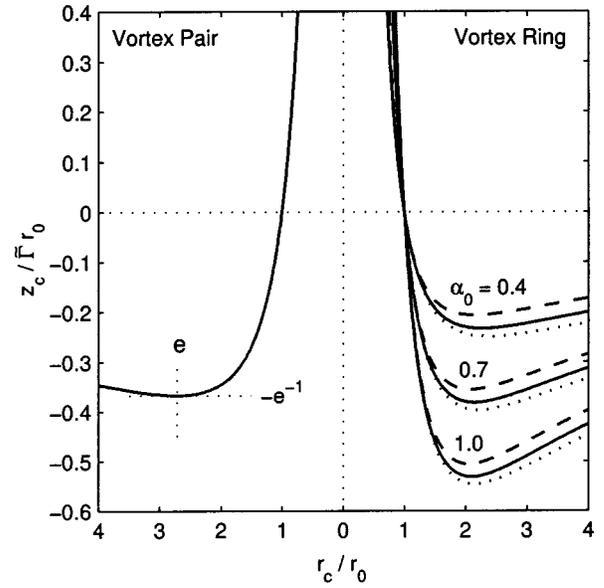
FIG. 2. Trajectory of the vortex pair (left) and vortex ring (right) in the (r,z) plane. The trajectory of the vortex ring is shown for different values of α_0, for $\mathrm{Re}_{v0} = 2$ (dashed), 8 (solid), and 80 (dotted). Note that the transverse coordinate is normalized with $\tilde{\Gamma} r_0$ whereas the axial coordinate is normalized with r_0.

$$\frac{dr_c}{dt} = A_0 r_c, \quad \frac{dz_c}{dt} = -A_0 z_c - \frac{\Gamma}{4\pi r_c}. \tag{6}$$

When these equations are integrated using as initial conditions the values r_0 and z_0 of the vortex position at $t=0$, we obtain the nondimensional vortex core position

$$r_c/r_0 = \xi_c = e^\tau, \quad z_c/r_0 = \eta_c = -\tilde{\Gamma}\tau e^{-\tau}, \tag{7}$$

which is shown in Fig. 2, written here in terms of the nondimensional time $\tau = A_0 t$ and the nondimensional coordinates $\xi = r/r_0$ and $\eta = z/r_0$. Here we have chosen as time origin the time of passage of the vortex pair through the original interface between the two streams.

Then, the ratio

$$\tilde{\Gamma} = \Gamma/4\pi r_0^2 A_0, \tag{8}$$

appearing in (7), equal to the ratio $V_{I0}/A_0 r_0$ of the characteristic self-induced velocity, $V_{I0} = \Gamma/4\pi r_0$, of the vortex pair to the radial velocity $A_0 r_0$ of the vortices, is the main parameter that characterizes the interaction of the vortex pair with the mixing layer.

If we measure the velocities with the scale $A_0 r_0$, the instantaneous velocity field, $\tilde{u} = u/A_0 r_0$, $\tilde{v} = v/A_0 r_0$, is given by

$$\tilde{u} = \xi - 2\tilde{\Gamma}\left[\frac{\eta - \eta_c}{(\xi - \xi_c)^2 + (\eta - \eta_c)^2} \right.$$
$$\left. - \frac{\eta - \eta_c}{(\xi + \xi_c)^2 + (\eta - \eta_c)^2} \right], \tag{9a}$$

$$\tilde{v} = -\eta + 2\tilde{\Gamma}\left[\frac{\xi - \xi_c}{(\xi - \xi_c)^2 + (\eta - \eta_c)^2}\right.$$
$$\left. - \frac{\xi + \xi_c}{(\xi + \xi_c)^2 + (\eta - \eta_c)^2}\right]. \tag{9b}$$

The position at various times of the mixing layer, which is infinitely thin in the limiting case, $\Gamma/\nu \gg 1$ and $A_0 r_0^2/\nu \gg 1$, that we are analyzing, corresponds to the time evolution of the fluid surface which at $\tau \to -\infty$ is at $\eta = 0$.

Thus, the centerplane value $\eta_m = z_m/r_0(<0)$ of this mixing layer, which corresponds to $\xi = 0$, is given from Eq. (9b) by

$$\frac{d\eta_m}{d\tau} = -\eta_m - \frac{4\tilde{\Gamma}\xi_c}{\xi_c^2 + (\eta_c - \eta_m)^2}, \tag{10}$$

where ξ_c and η_c are given by (7), complemented with the boundary condition $\eta_m = 0$ at $\tau \to -\infty$.

The time evolution of the nondimensional strain rate, $\tilde{A} = A/A_0$, at the lower point region of the mixing layer can be calculated using (9a) at $\eta = \eta_m$ and $\xi \ll \xi_c$. This gives

$$\tilde{A} = \frac{\tilde{u}}{\xi} = 1 + \frac{8\tilde{\Gamma}(\eta_c - \eta_m)\xi_c}{[\xi_c^2 + (\eta_c - \eta_m)^2]^2}, \tag{11}$$

which, as will be shown below, we need in order to calculate the time evolution of the mixing layer thickness and the scalar dissipation rate, which determines the time of extinction of the diffusion flame.

B. The axisymmetric case

The formulation of the problem is more involved in the case of the axisymmetric motion of a vortex ring in a counterflow. The self-induced velocity V_I of a vortex ring depends on the circulation, Γ, the radius of the vortex ring, r_c, and the apparent size, δ_v, of the vortex core, which in addition depends on the vorticity distribution, as discussed in detail by Saffman.[42]

For the self-induced velocity of a vortex ring we shall use the value

$$V_I = \frac{\Gamma}{4\pi r_c}\left(\log\frac{8r_c}{\delta_v} - C\right), \tag{12}$$

where the constant C depends on the shape of the vorticity distribution within the core. Here we shall use the value $C = 0.558$ corresponding to a Gaussian vorticity distribution,[42] as discussed in detail in the Appendix. The vortex core size is defined by

$$\delta_v^2 = \frac{2\pi}{\Gamma}\int_0^\infty \rho^3 \omega(\rho, t)d\rho \tag{13}$$

in terms of the instantaneous value of the vorticity $\omega(\rho, t)$ at a distance ρ from the vortex centroid. Then the dynamics of the vortex ring is given by

$$\frac{dr_c}{dt} = \frac{A_0}{2}r_c, \tag{14}$$

$$\frac{dz_c}{dt} = -A_0 z_c - \frac{\Gamma}{4\pi r_c}\left(\log\frac{8r_c}{\delta_v} - C\right). \tag{15}$$

Due to the stretching associated with the growth of the vortex ring radius, the size δ_v of the vorticity core will also change with time. If we neglect viscous diffusion, the volume of the vorticity core, proportional to $r_c\delta_v^2$, should remain constant, as is usually assumed in inviscid vortex rings models (e.g., Miloh and Shlien,[45] Miyazaki and Kambe,[46] Tyvand and Miloh[47]).

On the other hand, when the diffusion time δ_v/ν is of the order of the strain time A_0^{-1}, the distribution of vorticity in the vortex core will eventually reach a steady state characterized by a radial balance between convection and diffusion, leading to a constant value of the vortex core thickness of the order of the characteristic viscous length $(\nu/A_0)^{1/2}$.

In particular, if we measure the characteristic viscous time of the vortex core δ_v^2/ν with the characteristic strain time A_0^{-1} we obtain the Reynolds number

$$\mathrm{Re}_v = \frac{\delta_v^2 A_0}{\nu} = \left(\frac{\delta_v}{r_0}\right)^2 \mathrm{Re}_0, \tag{16}$$

which can also be viewed as the square of the nondimensional vortex core thickness based on the viscous length $(\nu/A_0)^{1/2}$. The time evolution of the vortex core size can only be determined from a detailed analysis of the vorticity dynamics within the core. This analysis, which is left to the Appendix, gives

$$\mathrm{Re}_v = 8 + (\mathrm{Re}_{v0} - 8)e^{-\tau/2} \tag{17}$$

where $\mathrm{Re}_{v0} = \delta_{v0}^2 A_0/\nu$ denotes the value of Re_v at $\tau = 0$.

Thus, to characterize the vortex ring we shall use its constant circulation Γ together with the values r_0 and δ_{v0} of the vortex ring radius r_c and the vortex core thickness δ_v when the vortex ring crosses, at time $t = 0$, the unperturbed position of the dividing surface $z = 0$ of the mixing layer.

Then, r_c and z_c will be given by the solution of (14) and (15) with the boundary conditions $r_c = r_0$ and $z_c = 0$ at $t = 0$, and with δ_v given by (16) and (17) as a function of time. This yields

$$r_c/r_0 = \xi_c = e^{\tau/2} \tag{18}$$

that can be used to write

$$\frac{d\eta_c}{d\tau} = -\eta_c - \frac{\Gamma}{4\pi r_0^2 A_0}e^{-\tau/2}\left\{2\pi\alpha_0 + \frac{\tau}{2} - \frac{1}{2}\log\left[\frac{8}{\mathrm{Re}_{v0}}\right.\right.$$
$$\left.\left. + \left(1 - \frac{8}{\mathrm{Re}_{v0}}\right)e^{-\tau/2}\right]\right\}. \tag{19}$$

Here we have introduced the parameter

$$\alpha_0 = \frac{V_{I0}}{\Gamma/2r_0} = \frac{1}{2\pi}\left(\log\frac{8r_0}{\delta_{v0}} - C\right) = \frac{1}{2\pi}\left(\log\frac{8\,\mathrm{Re}_0^{1/2}}{\mathrm{Re}_{v0}^{1/2}} - C\right), \tag{20}$$

or nondimensional form of the self-induced velocity V_{I0} at $\tau = 0$, which determines the structure of the flow when the vortex ring crosses the original plane of the mixing layer.

Equation (19) can be integrated with the boundary condition $\eta_c = 0$ at $\tau = 0$ to give

$$\frac{\eta_c}{\tilde{\Gamma}} = -\left[2\alpha_0 - \frac{1}{\pi} + \frac{1}{2\pi}\left(\tau - \log\frac{\mathrm{Re_v}}{\mathrm{Re_{v0}}}\right)\right]e^{-\tau/2}$$
$$+\left[2\alpha_0 - \frac{1}{\pi} + \frac{1}{2\pi}\left(\frac{\mathrm{Re_{v0}}}{8} - 1\right)\left(\frac{\tau}{2} + \log\frac{\mathrm{Re_v}}{\mathrm{Re_{v0}}}\right)\right]e^{-\tau}$$

(21)

where $\mathrm{Re_v}$ is given by Eq. (17) as a function of time in terms of its initial value $\mathrm{Re_{v0}}$ at $\tau = 0$. Figure 2 shows the trajectories of the vortex core in the plane (r, z) for different values of α_0 and $\mathrm{Re_{v0}}$.

In (21), the nondimensional vortex strength

$$\tilde{\Gamma} = \Gamma/2r_0^2 A_0$$

(22)

is the ratio of the characteristic turnover velocity of the vortex, $\Gamma/2r_0$, to the baseline strain velocity $A_0 r_0$ at a distance r_0 from the stagnation point. Alternatively, it can also be viewed as the ratio of the characteristic strain induced by the vortex ring, $\Gamma/2r_0^2$, to the basic strain, A_0, or as the ratio of the basic strain time, A_0^{-1}, to the turnover time, $2r_0^2/\Gamma$. It is important to note that the above definition of the nondimensional vortex circulation $\tilde{\Gamma}$ differs from that of the two-dimensional case by a factor of 2π.

In the following, we shall restrict our attention to values of α_0 smaller than unity, which corresponds to values of $\delta_v/r_c \gtrsim 1/117$ for which the domain of fluid traveling with the vortices remains bubble shaped,[42] as is typically observed in the experiments.

To calculate the instantaneous velocity field at any point (r, z) other than (r_c, z_c), we need to add to the unperturbed velocity field, $u = rA_0/2$ and $v = -zA_0$, the velocity field induced by the vortex ring. Then, the nondimensional velocity field can be written as[48]

$$\tilde{u} = \frac{\xi}{2} - \frac{\tilde{\Gamma}}{\pi\xi_c}\left(\frac{\xi_c}{2\xi}\right)^{3/2}\left(\frac{\eta - \eta_c}{\xi_c}\right)I_1(\mu),$$

(23a)

$$\tilde{v} = -\eta + \frac{\tilde{\Gamma}}{\pi\xi_c}\left(\frac{\xi_c}{2\xi}\right)^{3/2}\left[\frac{\xi}{\xi_c}I_1(\mu) - I_0(\mu)\right],$$

(23b)

where I_0 and I_1 can be expressed in terms of K and E, the complete elliptic integrals of the first and the second kind, as

$$I_0(\mu) = \int_0^\pi \frac{d\theta}{1 + \mu - \cos\theta} = \frac{2/\mu}{(2+\mu)^{1/2}}E(k),$$

(24)

$$I_1(\mu) = \int_0^\pi \frac{\cos\theta\, d\theta}{1 + \mu - \cos\theta}$$

$$= \frac{2}{(2+\mu)^{1/2}}\left[\frac{1+\mu}{\mu}E(k) - K(k)\right],$$

(25)

with

$$\mu = \frac{(\eta - \eta_c)^2 + \xi^2 + \xi_c^2}{2\xi\xi_c} - 1,$$

(26)

$$k = \left(\frac{2}{2+\mu}\right)^{1/2}.$$

(27)

In particular, the vertical evolution $\eta_m = z_m/r_0$ of the mixing layer in the near-axis region, where $r \ll r_c$, is given by the integration of

$$\frac{d\eta_m}{d\tau} = -\eta_m - \frac{\tilde{\Gamma}\xi_c^2}{[\xi_c^2 + (\eta_c - \eta_m)^2]^{3/2}},$$

(28)

where ξ_c and η_c are given by (18) and (21), with the initial condition $\eta_m = 0$ at $\tau \to \infty$, which provides, together with Eq. (21), the evolution of the strain rate experienced by the mixing layer at the axis of symmetry

$$\tilde{A} = \frac{A}{A_0} = 1 + \frac{3\tilde{\Gamma}\xi_c^2(\eta_c - \eta_m)}{[\xi_c^2 + (\eta_c - \eta_m)^2]^{5/2}}.$$

(29)

IV. STRUCTURE OF THE MIXING LAYER

A. Conservation equations and thermochemical model

In the Burke–Schumann limit of infinitely fast chemistry the fuel and oxygen do not coexist. Their mass fractions Y_F and Y_{O_2}, which satisfy the relation $Y_F \cdot Y_{O_2} = 0$, can be calculated, if we assume equal diffusivities of mass and heat D_T, in terms of the mixture fraction Z, which is defined by

$$Z = \frac{SY_F/Y_{F0} - Y_{O_2}/Y_{O_20} + 1}{S + 1}$$

(30)

in terms of the mass fractions of fuel and oxygen at their corresponding feeding streams, Y_{F0} and Y_{O_20}, and the air to fuel mass stoichiometric ratio $S = s_O Y_{F0}/Y_{O_20}$, where s_O denotes the mass of oxygen consumed per unit mass of fuel. Then the temperature T, given by $T = T_0 + \gamma T_0(1 - Y_F/Y_{F0} - Y_{O_2}/Y_{O_20})$, can also be obtained in terms of the mixture fraction, where T_0 is the temperature of the feeding streams, and γ is the heat release parameter, defined by $\gamma = qY_{F0}/[c_pT_0(1+S)]$ in terms of the heat release q per unit mass of fuel consumed, and the specific heat c_p at constant pressure, assumed here to be constant.

If we assume, in addition, constant values for the gas density ρ and the thermal diffusivity D_T, the conservation equation for the mixture fraction Z can be written as

$$\frac{\partial Z}{\partial t} + \mathbf{u} \cdot \nabla Z = D_T \nabla^2 Z,$$

(31)

where the velocity field $\mathbf{u} = (u, v)$ is given by (9) in the two-dimensional case and by (23) in the axisymmetric case. This equation is to be solved with the boundary conditions $Z = 0$ in the oxidizer stream and $Z = 1$ in the fuel stream, and then the flame sheet is given by $Z = Z_s = 1/(S+1)$.

B. Asymptotic solution for large Peclet numbers

To describe the distribution of the mixture fraction in the mixing layer when the Reynolds number $A_0 r_0^2/\nu$ is large, we define a system of orthogonal curvilinear coordinates (s, n) attached to it, as shown in Fig. 1. Here s and n denote the distances measured along and normal to the mixing layer, respectively, with the origin of s located at $r = 0$.

In the coordinate system attached to the mixing layer, the continuity equation takes the form

$$\frac{\partial(r^j u_s)}{\partial s}+\frac{\partial(r^j u_n)}{\partial n}=0, \tag{32}$$

where $j=0$ in the two-dimensional case and $j=1$ in the axisymmetric case, and u_s and u_n denote the local velocity components along the s and n axis.

Since the density is assumed to be constant, the term $\partial(r^j u_s)/\partial s$ takes a constant value across the mixing layer. Then, Eq. (32) can be integrated with the boundary condition $u_n=0$ at $n=0$ to give

$$u_n=-nA(s,t), \tag{33}$$

where

$$A(s,t)=\frac{1}{r^j}\frac{\partial(r^j u_s)}{\partial s} \tag{34}$$

is the local strain rate imposed by the flow on the mixing layer, to be discussed in Sec. V below, and Eq. (31) can be written as

$$\frac{\partial Z}{\partial t}+u_s\frac{\partial Z}{\partial s}-nA\frac{\partial Z}{\partial n}=D_T\frac{\partial^2 Z}{\partial n^2}. \tag{35}$$

The solution of this equation must be symmetric, and analytic, at $s=0$, and satisfy the boundary conditions $Z=0$ as $n\to\infty$ and $Z=1$ as $n\to-\infty$.

It should be noted that in Eq. (35) we have dropped out the effects of curvature, which are of order $Pe_0^{-1/2}\ll1$. Here $Pe_0=A_0 r_0^2/D_T$ denotes the Peclet number of the unperturbed flow, which is large when $A_0 r_0^2/\nu$ is large since the Prandtl number $Pr=\nu/D_T$ is of order unity for gases. Similarly, we have neglected the longitudinal diffusion term, of order Pe_0^{-1}, which is even smaller than the curvature terms.

According to this, when the characteristic size of the vortex pair or ring is large compared with the mixing layer thickness, the effects of the curvature are negligible and, in first approximation, the mixing layer behaves as quasi-planar. This is in agreement with the experimental results of Santoro,[35] corresponding to fuels with unity Lewis number, which show that the scalar dissipation rate at extinction is independent of the radius of the vortex in the case of vortex rings large compared to the original thickness of the mixing layer.

It is easy to check that the solution of (35) has the self-similar form $Z(n,s,t)=Z_0(\eta)$, where $\eta=n/\delta_m(s,t)$ is a similarity variable[8,49] defined by measuring the distance normal to the mixing layer with the local value $\delta_m(s,t)$ of the mixing layer thickness, to be given by Eq. (38) below. Written in terms of the new variables, (35) takes the form

$$-\eta\frac{dZ_0}{d\eta}\left[\frac{1}{\delta_m}\left(\frac{\partial\delta_m}{\partial t}+u_s\frac{\partial\delta_m}{\partial s}\right)+A\right]=\frac{D_T}{\delta_m^2}\frac{d^2 Z_0}{d\eta^2}. \tag{36}$$

This equation is satisfied if $\delta_m(s,t)$ and $Z_0(\eta)$ are chosen so as to verify the equations[50]

$$\eta Z_{0\eta}+Z_{0\eta\eta}=0, \tag{37}$$

corresponding to a mixing layer subject to a constant unit strain, where the subscript η indicates derivative, and

$$\frac{\partial\delta_m^2}{\partial t}+u_s\frac{\partial\delta_m^2}{\partial s}=2D_T-2A\,\delta_m^2, \tag{38}$$

obtained equating the bracketed term in Eq. (36) to D_T/δ_m^2 and multiplying the resulting equation by $2\,\delta_m^2$.

The solution of (37) with the boundary conditions $Z_0(\infty)=Z_0(-\infty)-1=0$ is

$$Z_0(\eta)=(\tfrac{1}{2})\mathrm{erfc}(\eta/\sqrt{2}), \tag{39}$$

a mixture fraction whose dependence on s and t is through the local value $\delta_m(s,t)$ of the thickness of the mixing layer, given by Eq. (38). This equation can be solved for δ_m^2 with the method of characteristics using the initial condition $\delta_m^2=\delta_{m0}^2=D_T/A_0$ at $t\to-\infty$ provided by the solution of the unperturbed problem.

With $Z_0(\eta)$ given by Eq. (39), the flame surface lies, in first approximation, at $\eta=\eta_s$, where $Z_0=Z_{0s}=1/(S+1)$, given implicitly by $Z_{0s}=(\tfrac{1}{2})\mathrm{erfc}(\eta_s/\sqrt{2})$. The nondimensional mixture fraction gradient at $Z_0=Z_{0s}$ is

$$\kappa(S)\equiv|Z_{0\eta}|_s=(2\pi)^{-1/2}\exp(-\eta_s^2/2), \tag{40}$$

a value that depends only on S and, therefore, does not vary along the flame surface. This value can be used to calculate the value $\chi_s=D_T|\nabla Z|_s^2$ of the scalar dissipation rate at the stoichiometric surface, given in nondimensional form by

$$\chi_s/\chi_{s0}=\delta_{m0}^2/\delta_m^2 \tag{41}$$

where $\chi_{s0}=A_0\kappa(S)$ is the scalar dissipation rate at the unperturbed flame.

The analysis provides also the mass of fuel burned per unit surface per unit time, m_f, proportional to $|\nabla Z|_s$, which can be written in nondimensional form as

$$m_f/m_{f0}=\delta_{m0}/\delta_m, \tag{42}$$

where $m_{f0}=\rho Y_{F0}(D_T A_0)^{1/2}(1+S^{-1})\kappa(S)$ is the corresponding fuel consumption rate at the unperturbed flame.

V. NUMERICAL RESULTS

To describe the distortion of the mixing layer it is convenient to introduce the Lagrangian parameter λ and parametrize the perturbed mixing layer as $\mathbf{x}(\lambda;t)=(r(\lambda;t),z(\lambda;t))$. Then, the local strain rate experienced by the mixing layer, given by $A=-\mathbf{n}\cdot\mathcal{S}\cdot\mathbf{n}$, can be expressed in nondimensional form as

$$\tilde{A}=\frac{A}{A_0}=\frac{-\tilde{u}_\xi\eta_\lambda^2+(\tilde{u}_\eta+\tilde{v}_\xi)\xi_\lambda\eta_\lambda-\tilde{v}_\eta\xi_\lambda^2}{\xi_\lambda^2+\eta_\lambda^2}, \tag{43}$$

where $\mathbf{n}$ denotes the unit normal vector and $\mathcal{S}$ the velocity gradient tensor, and the subscripts ξ, η, and λ identify partial derivatives.

This expression involves the velocity gradients with respect to ξ and η, as well as the derivatives of the coordinates ξ and η with respect to the Lagrangian parameter. The former can be obtained analytically, in the two-dimensional
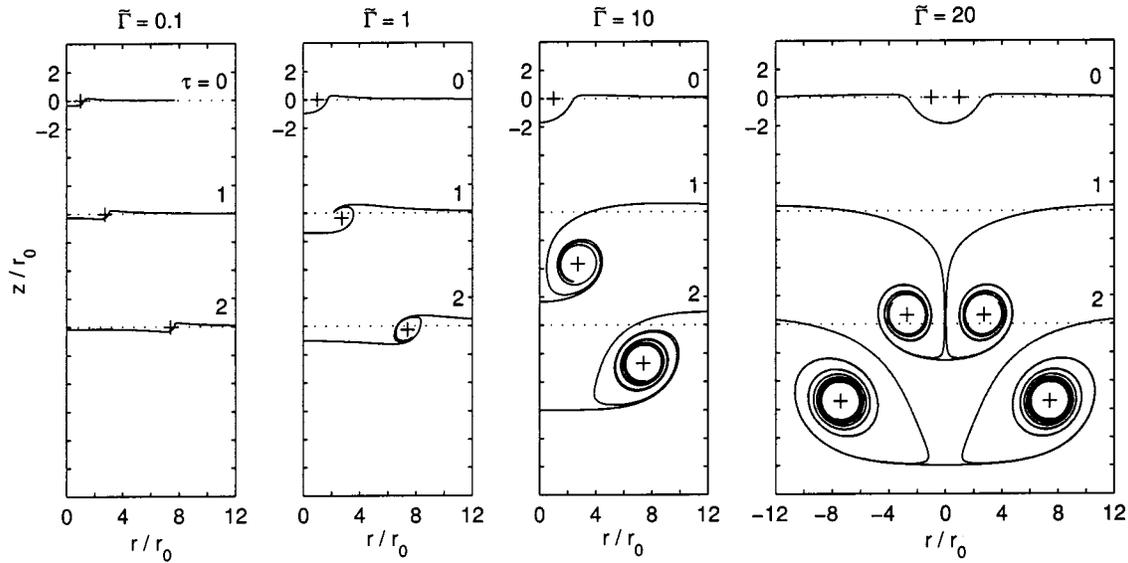
FIG. 3. Position at various times of the two-dimensional mixing layer for different values of $\tilde{\Gamma}$. The plane $z=0$ (dotted lines) has been displaced downwards to avoid superposition of the plots. The vortex cores are represented by a $+$ sign.

case, or numerically, in the axisymmetric case, while the latter must be obtained by numerical integration of the problem

$$\frac{d}{d\tau} \begin{Bmatrix} \xi \\ \eta \\ \xi_\lambda \\ \eta_\lambda \end{Bmatrix} = \begin{Bmatrix} \tilde{u} \\ \tilde{v} \\ \tilde{u}_\xi \xi_\lambda + \tilde{u}_\eta \eta_\lambda \\ \tilde{v}_\xi \xi_\lambda + \tilde{v}_\eta \eta_\lambda \end{Bmatrix}, \tag{44}$$

where $d/d\tau$ denotes material derivative, with the initial conditions $\xi=f(\lambda)$, $\eta=0$, $\xi_\lambda=f'(\lambda)$, and $\eta_\lambda=0$ at $-\tau=-\tau_0 \gg \min(\tilde{\Gamma}^{-1},1)$. In this case a natural choice for the parametrization is to take $f(\lambda)=e^\lambda$, which defines the Lagrangian parameter λ as the natural logarithm of the radial coordinate at $\tau=\tau_0$.

This procedure yields the position of the mixing layer and the local strain rate experienced by it as a function of time, what allows us to integrate the nondimensional form of Eq. (38), namely

$$\frac{d\delta^2}{d\tau} = 2 - 2\tilde{A}\delta^2, \tag{45}$$

subject to the initial condition $\delta^2=1$ as $\tau \to -\infty$. From this we may calculate the evolution of the mixing layer thickness and, using Eqs. (41) and (42), the values of the scalar dissipation rate and the fuel consumption rate, respectively.

The numerical results, presented in Figs. 3–5, to be discussed below, were obtained using an adaptive Cash–Karp[51] Runge–Kutta method with variable step size, based on embedded Runge–Kutta formulas of fourth and fifth order, as outlined by Press *et al.*[52] (p. 708). The number of points used in the description of the mixing layer ranged from 1000 to 4000, and the tolerance of the results was maintained at four-digit accuracy.

A. Two-dimensional case

Figure 3 shows the location of the two-dimensional mixing layer at various times for different values of $\tilde{\Gamma}$. The displacement of the mixing layer below its original plane, when measured with r_0, remains small at all times for small values of $\tilde{\Gamma}$. This displacement grows linearly with $\tilde{\Gamma}$, and the interface becomes strongly wrapped around the vortices when $\tilde{\Gamma}$ is moderately large compared with unity.

The structure of the mixing layer at various times is shown in Fig. 5(a) in the case $\tilde{\Gamma}=10$, showing the mixing layer thickness in arbitrary units as well as the position of the local maxima and minima of the strain and scalar dissipation rates. It should be noted that while the peak scalar dissipation rate is found at the center plane during the initial stages of the interaction, it finally shifts to a radius of order r_c, with peak values slightly higher than those encountered along the center plane.

As discussed by Marble,[16] during the roll-up process observed in Figs. 3–5, the adjacent flame sheets begin to interact as soon as the mixing layer thickness becomes of the order of the spacing between the flame surfaces. As the subsequent diffusion between adjacent flame elements depletes the concentration of reactants, the reactant consumption rate decreases, reducing the risk of local extinction, until the two flame sheets eventually annihilate each other. This leads to the formation of pockets of unburned reactants surrounded by diffusion flames,[53] which increases the effective flame area and enhances the overall combustion process.[38]

As can be seen, previous to this roll-up process the mixing layer is strongly deformed in the rear part of the vortices, eventually developing a sharp bend, where, obviously, the assumption of negligible curvature leading to Eq. (35) ceases to be valid. It should be noted, however, that in this region the mixture fraction gradients are expected to decrease, as discussed above, thus reducing the possibility of extinction
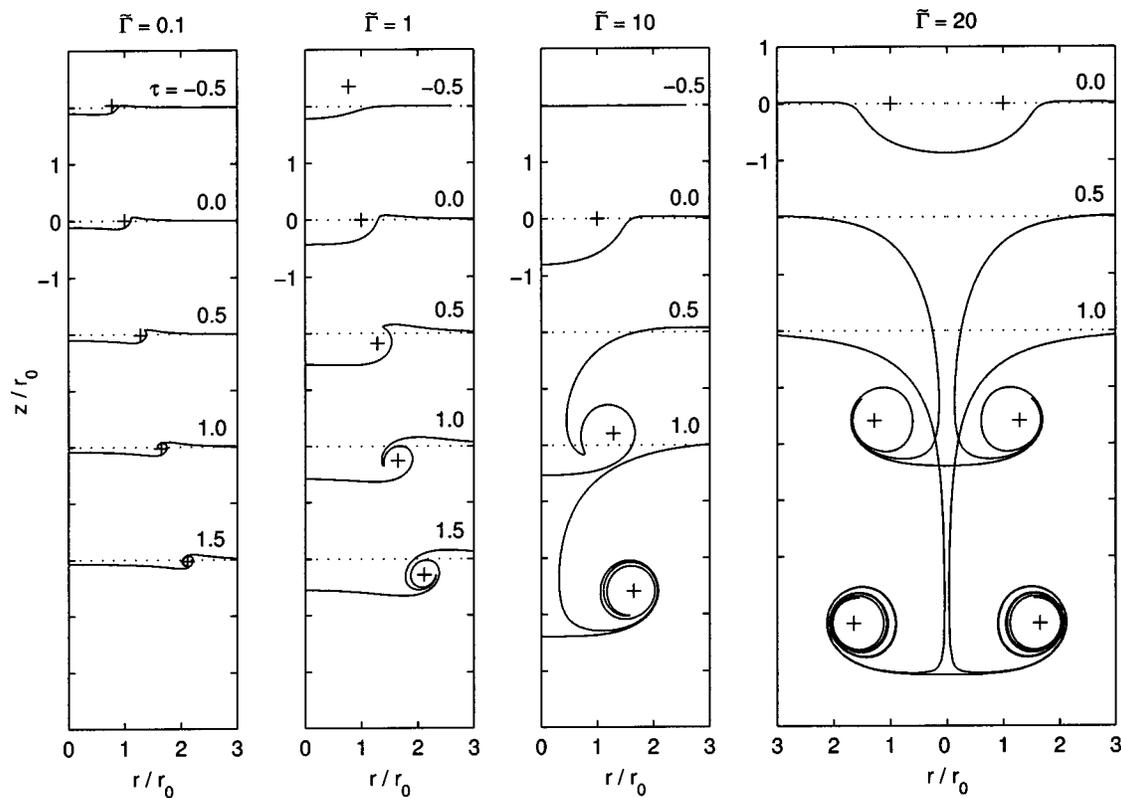
FIG. 4. Position at various times of the axisymmetric mixing layer for $\alpha_0 = 0.5$, $Re_{v0} = 8$, and different values of $\widetilde{\Gamma}$. The plane $z = 0$ (dotted lines) has been displaced downwards to avoid superposition of the plots. The vortex cores are represented by a $+$ sign.

in agreement with the experimental observations (see, for example, Ref. 30). Nevertheless, the local failure of our analysis in this region does not invalidate its applicability to the forward part of the bubble, where all the assumptions made are still valid. In fact, due to the increased values of the local strain rate the mixing layer becomes even thinner in this region, thus allowing us to neglect curvature effects with more reason. This is in agreement with most of the previous theoretical, numerical, and experimental work, which shows that the critical conditions for local flame extinction occur in the region ahead of the vortices (although not necessarily at the forward stagnation point), where the analysis presented here is valid.

Figures 6(a)–6(c) show the time evolution of the peak scalar dissipation rate along the mixing layer together with its center plane value as a function of time for different values of $\widetilde{\Gamma}$. In fact, in order to use the same scale in all the plots, which makes the comparison of results easier, the figures show the inverse of the scalar dissipation rate, proportional to the square of the mixing layer thickness. As can be seen, except for small values of $\widetilde{\Gamma}$ the absolute maximum of the scalar dissipation rate is only slightly higher (about a 4%) than its maximum value at the center plane. Thus, we may conclude that in the two-dimensional case the center plane solution could be used to predict the conditions for local flame extinction accurately. Note also the delay and attenuation of the scalar dissipation rate with respect to the imposed strain due to unsteady effects.

The perturbations induced by the vortices extend to distances of order $\widetilde{\Gamma}^{1/2} r_0$ from the vortex core, which are small

compared with r_0 when $\widetilde{\Gamma}$ is small. In this case the perturbations are much more important in the vicinity of the vortices, where the scalar dissipation reaches its maximum value, than in the symmetry plane.

B. Axisymmetric case

In the axisymmetric case the solution depends also on the effective value δ_v of the vortex core size through the self-induced propagation velocity of the vortex ring. As previously discussed, the time evolution of the vortex core size is given by the detailed analysis of the vorticity core dynamics presented in the Appendix. This analysis shows that the vortex core size $\delta_v = (Re_v \nu / A_0)^{1/2}$ tends for large times to a constant value determined by the radial competition between convection and diffusion, which corresponds to $Re_v = 8$. Here Re_v represents the Reynolds number based on the vortex core size δ_v, the characteristic strain velocity $A_0 \delta_v$, and the kinematic viscosity ν.

In what follows we shall assume that the dynamics of the vortex core is such that the vortex core size is constant, which corresponds to the case $Re_v \equiv Re_{v0} = 8$. It should be noted that the assumption that δ_v is constant is not critical, since as shown by Eq. (12) the influence of δ_v on the self-induced propagation velocity is logarithmic, and therefore the variations of δ_v will have very little effect on the interaction process. This is especially true for $\widetilde{\Gamma} \gg 1$, when the time scale of the interaction is much shorter than the characteristic strain time, and the vortex core size, whose variations
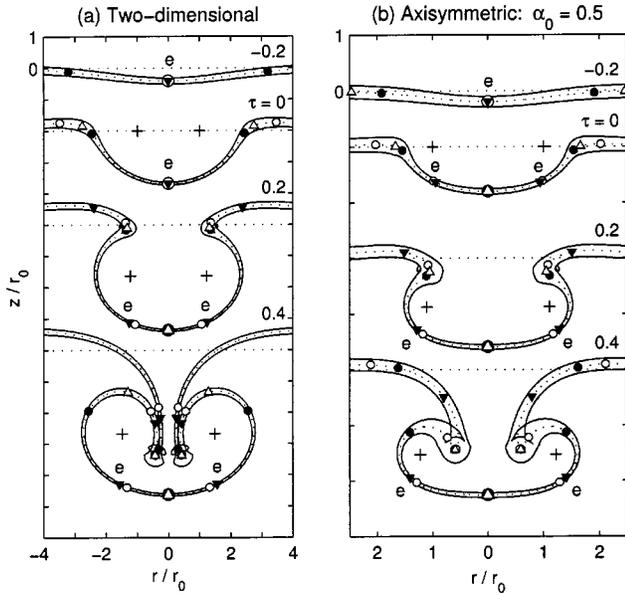
FIG. 5. Structure at various times of the two-dimensional and axisymmetric mixing layers corresponding to $\tilde{\Gamma}=10$, $\alpha_0=0.5$, and $\mathrm{Re}_{v0}=8$, showing the thickness of the mixing layer in arbitrary units and the local maxima/minima of the strain rate (scalar dissipation rate) as hollow/solid circles (solid/ hollow triangles). The location of the maximum scalar dissipation rate at each time is indicated by an "e" denoting extinction point. The plane $z=0$ has been displaced downwards to avoid superposition of the plots.

occur in times of order A_0^{-1}, can be taken as constant during the interaction.

Figure 4 shows the location of the axisymmetric mixing layer at various times for $\alpha_0=0.5$ and different values of $\tilde{\Gamma}$. As can be seen, the effect of the nondimensional vortex strength is similar to that of the two-dimensional case. The structure of the mixing layer at various times is shown in Fig. 5(b) in the case $\alpha_0=0.5$ and $\tilde{\Gamma}=10$.

Figures 6(e)–6(i) show the peak value of the scalar dissipation rate as a function of time along with its value at the symmetry axis for $\alpha_0=0.5$, $\alpha_0=0.7$, and different values of $\tilde{\Gamma}$. In this case, as the interaction proceeds the peak scalar dissipation rate shifts from the axis to an annular region at a distance of order r_c away from the axis, where the peak scalar dissipation rate reaches its absolute maximum. However, this maximum value is now appreciably larger than the maximum scalar dissipation rate at the symmetry axis. As a consequence, we may conclude that in the axisymmetric case the analysis of the near-axis region could fail to predict the conditions for local flame extinction.

In particular, while sufficiently strong vortices could be able to extinguish the flame at the axis, weaker vortices could not be able to extinguish the flame there but would still be able to extinguish it in the annular region where the peak value of the scalar dissipation rate is reached. This may contribute to explaining the unexpected annular quenching regime observed by Katta et al.[30] for moderately strong vortices, which contrasts with the usual quenching at the axis of symmetry observed for stronger vortices.

As a final remark, it should be noted that due to the instability of the vortex ring to azimuthal bending waves, the

results presented herein are limited to values of the Reynolds number $A_1\delta_v^2/\nu$, based on the vortex core size, δ_v, and the self induced strain, A_I, experienced by the core, below a certain critical value (about 60; see Refs. 54 and 55 for details). Using the expression for the self-induced strain given by Saffman[55] [Eq. (4.2)], this leads to the approximate stability criterion

$$\tilde{\Gamma}\lesssim\frac{4}{3}\frac{60}{\mathrm{Re}_{v0}(\alpha_0-C')} \tag{46}$$

where $C'=(\frac{17}{12}-C)/2\pi$ is a constant equal to 0.186 for a uniform vorticity distribution and 0.137 for a Gaussian vorticity core. It is easy to check that all the results presented in Figs. 4–6 verify this condition.

It should be pointed out that the stability criterion (46) does not include the effect of the azimuthal stretching experienced by the core due to the growth of the vortex ring radius. This is believed to act as a stabilizing effect, so that the range of applicability of our analysis predicted by Eq. (46) should be viewed as conservative.

C. Summary of results

Figure 7 summarizes the results in terms of the maximum scalar dissipation rate experienced by the flame throughout the interaction. As can be seen, in the planar case the maximum scalar dissipation rate is well predicted by the centerplane solution for values of $\tilde{\Gamma}$ of order unity or large compared to unity. On the other hand, in the axisymmetric case the maximum scalar dissipation rate is substantially higher than that found at the axis, a difference that increases with α_0. The picture also shows the asymptotic behavior for large and small values of $\tilde{\Gamma}$ obtained in the following sections, which is in very good agreement with the numerical results.

VI. THE INTERACTION OF MIXING LAYERS WITH STRONG VORTICES ($\tilde{\Gamma}\gg1$)

The distortion of counterflow mixing layers by strong vortex pairs or vortex rings involves three different stages due to the great disparity of the time scales involved in the problem when $\tilde{\Gamma}\gg1$, as seen in Figs. 6(c), 6(f), and 6(i).

During the first stage, with a time scale of the order of the vortex turn over time, $\tilde{\Gamma}^{-1}A_0^{-1}$, the vortices cross the original plane of the mixing layer, which is strongly distorted and eventually becomes wrapped around the bubble of fluid that is transported by the vortices. During this stage, the strain rate, A, and the scalar dissipation rate, χ_s, rise to peak values of order $\tilde{\Gamma}A_0$, although the scalar dissipation presents an attenuation and a delay of order $\tilde{\Gamma}^{-1}A_0^{-1}$ due to unsteady effects, which in the case of the vortex ring depends on δ_{v0}/r_0. As can be seen, this is the most critical stage for local flame extinction.

In a second stage, with a characteristic time scale of the order of the strain time, A_0^{-1}, the stagnation point values of the strain and scalar dissipation rates decrease to their original, unperturbed values. During this stage the mixing layer becomes strongly wrapped around the vortices, while the core to core distance, or vortex ring radius, grows due to the
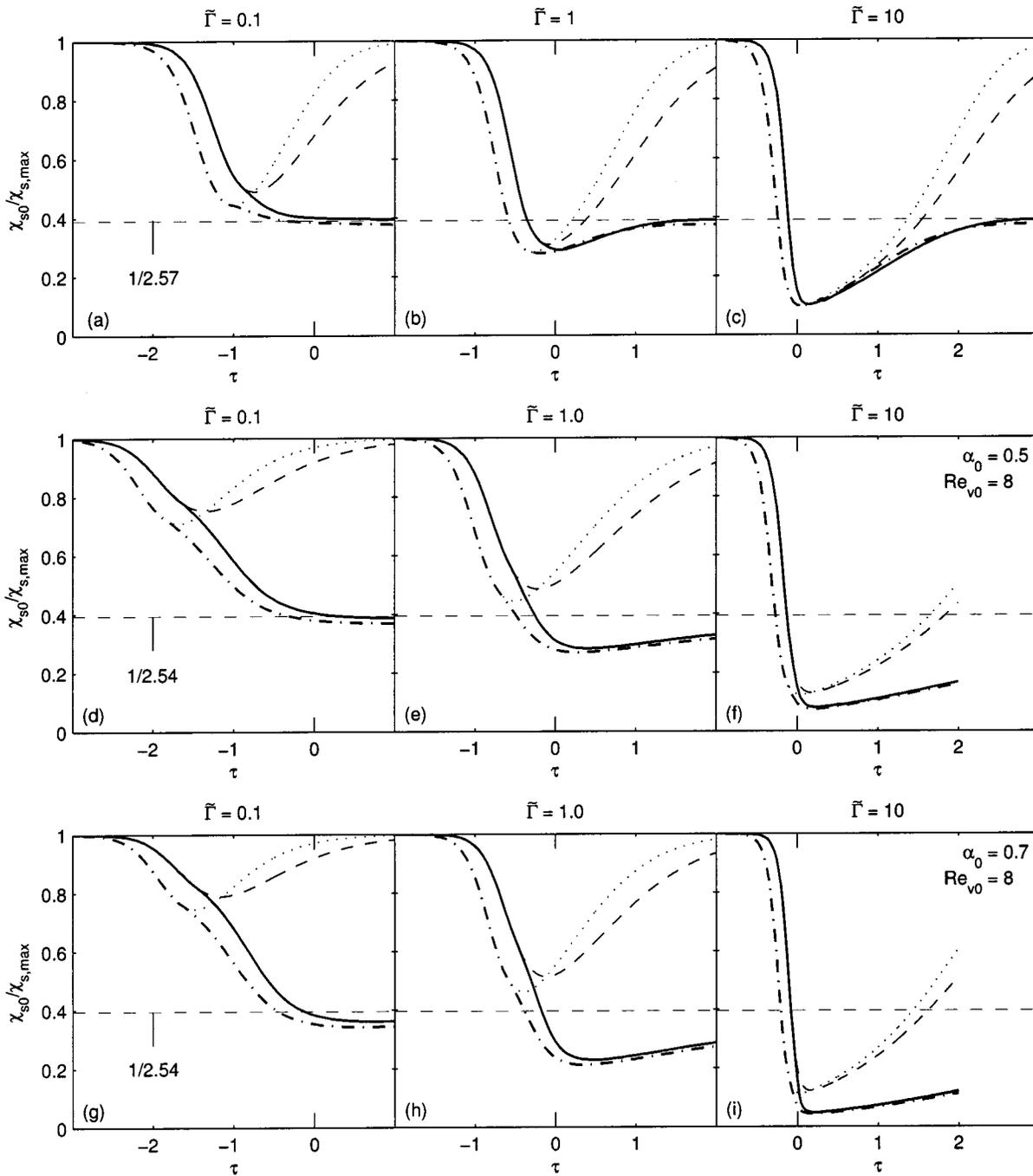
FIG. 6. Maximum value of the scalar dissipation rate (solid lines) and value of the scalar dissipation rate at the center plane/symmetry axis (dashed lines) as a function of time for different values of $\tilde{\Gamma}$ along with their corresponding quasi-steady values, the maximum strain rate (dot-dashed lines) and the strain rate at the center plane/symmetry axis (dotted lines): (a)–(c) two-dimensional case; (d)–(f) axisymmetric case for $\alpha_0 = 0.5$, $Re_{v0} = 8$; (g)–(i) axisymmetric case for $\alpha_0 = 0.7$, $Re_{v0} = 8$. The asymptotic value for large times is indicated by a horizontal dashed line.

basic strain. This reduces the self-induced velocity of the vortices, which are eventually convected back to the stagnation plane after reaching distances of order $z/r_0 \sim \tilde{\Gamma}$ below the original plane of the mixing layer.

For $\tau \gg 1$ the core to core distance, or vortex ring radius, becomes exponentially large. Then, in a reference frame moving with the vortex the velocity field becomes stationary, and the mixing layer adopts the form of the dividing streamlines emerging from local stagnation points, near the vorti-

ces. A detailed analysis of this stage, which differently from the first and second stages is present for all values of $\tilde{\Gamma}$, will be given in Sec. VII.

A. Analysis of the first stage of the interaction

During the first stage of the interaction the basic strain has a negligible effect on the distortion of the mixing layer (compared to the effect of the unsteady strain induced by the
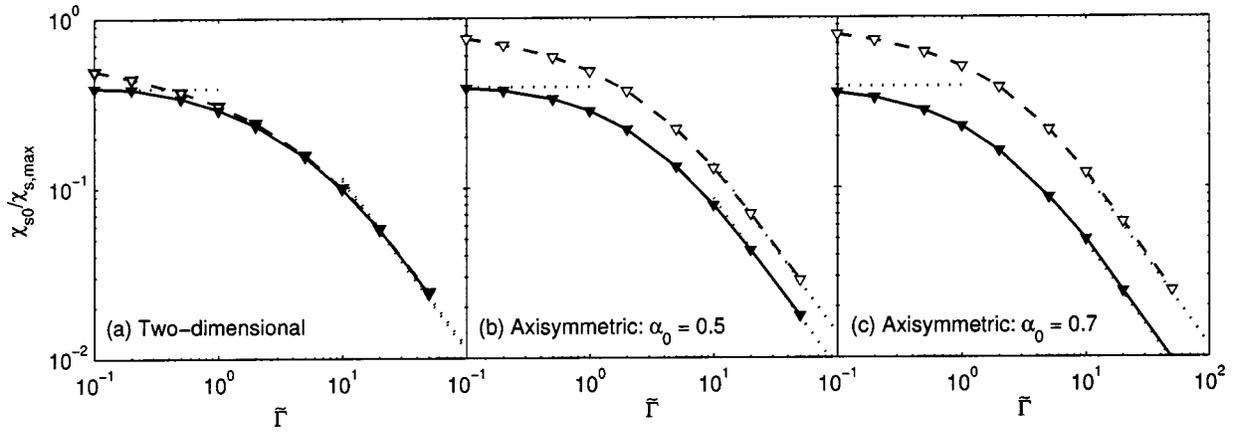
FIG. 7. Maximum scalar dissipation rate experienced along the mixing layer (solid lines) and maximum scalar dissipation rate at the center plane/symmetry axis (dashed lines) as a function of $\tilde{\Gamma}$: (a) two-dimensional case; (b), (c) axisymmetric case for $\mathrm{Re}_{v0}=8$ corresponding respectively to $\alpha_0=0.5$ and 0.7. The leading-order asymptotic predictions determined in Secs. VI A and VII are also indicated (dotted lines).

vortices) and the problem reduces in first approximation to the distortion of a fluid surface by a vortex pair, or vortex ring, impinging normal to it.

In a reference frame moving with the vortices the flow field is steady and, as can be seen in Fig. 8, the initially flat mixing layer becomes wrapped around the vortices in a time of the order of the vortex turnover time, $t_c=2\pi r_0^2/\Gamma$, eventually adopting the form of the dividing streamline. This allows us to evaluate the nondimensional strain rate at the forward stagnation point, $\hat{A}_{st}=A_{st}t_c$, and from it the nondimensional thickness of the mixing layer there, $\hat{\delta}_{st}^2 = \delta_{m,st}^2/D_T t_c = \hat{A}_{st}^{-1}$.

Here we shall use $\hat{\xi}=\xi=r/r_0$, $\hat{\eta}=\eta-\eta_c=(z-z_c)/r_0$, $\hat{\tau}=t/t_c$, $\hat{u}=u/(\Gamma/2\pi r_0)$, $\hat{v}=v/(\Gamma/2\pi r_0)$, and $\hat{\delta}=\delta_m/(D_T t_c)^{1/2}$ as dimensionless variables, with the nondimensional strain rate given by

$$\hat{A}=At_c=\frac{-\hat{v}^2\hat{u}_{\hat{\xi}}+\hat{u}\hat{v}(\hat{v}_{\hat{\xi}}+\hat{u}_{\hat{\eta}})-\hat{u}^2\hat{v}_{\hat{\eta}}}{\hat{u}^2+\hat{v}^2}. \quad (47)$$

Then, the integration of the problem

$$\frac{d}{d\hat{\tau}}\left\{\begin{array}{c}\hat{\xi}\\ \hat{\eta}\\ \hat{\delta}^2\end{array}\right\} = \left\{\begin{array}{c}\hat{u}\\ \hat{v}\\ 2-2\hat{A}\hat{\delta}^2\end{array}\right\} \quad (48)$$

with the initial conditions $\hat{\xi}=\hat{\xi}_0\ll 1$, $\hat{\eta}=\hat{\eta}_{st}$, and $\hat{\delta}^2=\hat{\delta}_{st}^2$ at $\hat{\tau}=0$ provides the evolution of the mixing layer thickness along the dividing streamline, which yields the maximum scalar dissipation rate at the flame surface

$$\chi_{s0}/\chi_{s,max}=(\delta_{m,min}/\delta_{m0})^2=\hat{\delta}_{min}^2 B\tilde{\Gamma}^{-1}, \quad (49)$$
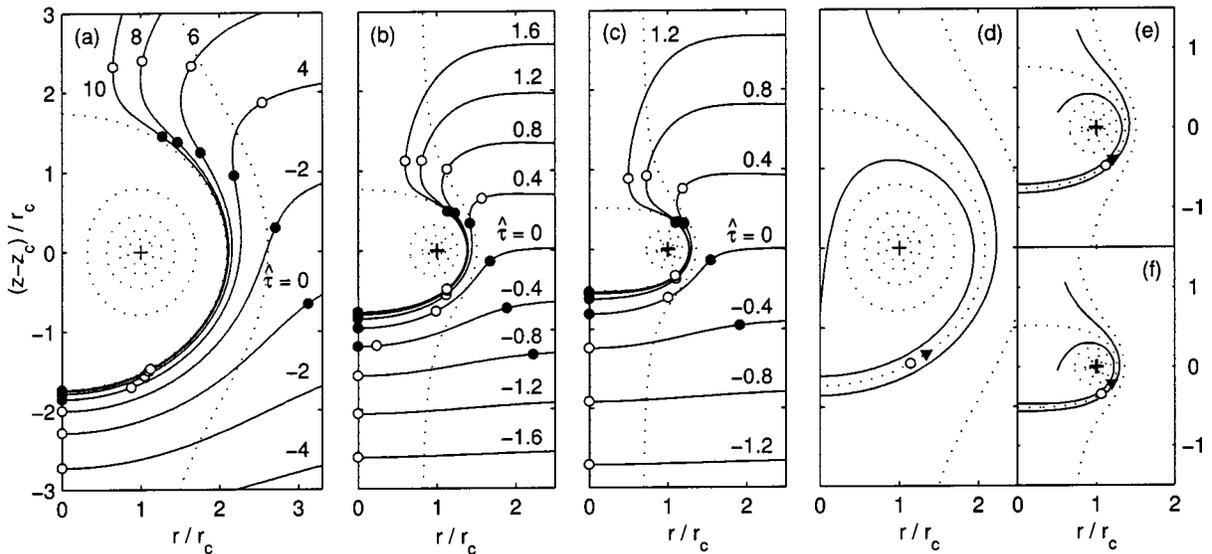
FIG. 8. (a)–(c) Distortion at various nondimensional times $\hat{\tau}=t/(2\pi r_c^2/\Gamma)$ of an initially flat fluid surface (solid lines) by freely propagating vortex pairs and vortex rings impinging normal to it: (a) vortex pair; (b), (c) vortex ring, corresponding to (b) $\alpha_0=0.5$ and (c) $\alpha_0=0.7$. The local maxima (minima) of the strain rate are indicated by hollow (solid) circles. (d)–(f) Structure of the mixing layer that develops between the fluid traveling with the vortices and the ambient fluid: (d) vortex pair; (e), (f) vortex ring, corresponding to (e) $\alpha_0=0.5$ and (f) $\alpha_0=0.7$. The points of maximum strain (hollow circles) and minimum mixing layer thickness (solid triangles) are clearly indicated. The mixing layer thickness is plotted using the same scale in all the plots.

where $B = \frac{1}{2}$ in the planar case and $B = \pi$ in the axysimmetric case.

1. Two-dimensional case

In the two-dimensional case $\hat{\eta}_{st} = -3^{1/2}$, $\hat{\delta}_{st}^2 = 4/3^{1/2} \simeq 2.31$, and the velocity field is given by

$$\hat{u} = -\frac{\hat{\eta}}{(\hat{\xi}-1)^2 + \hat{\eta}^2} + \frac{\hat{\eta}}{(\hat{\xi}+1)^2 + \hat{\eta}^2}, \tag{50}$$

$$\hat{v} = \frac{\hat{\xi}-1}{(\hat{\xi}-1)^2 + \hat{\eta}^2} - \frac{\hat{\xi}+1}{(\hat{\xi}+1)^2 + \hat{\eta}^2} + \frac{1}{2}. \tag{51}$$

The structure of the mixing layer obtained from the integration of (48) with the above velocity field is shown in Fig. 8(d). The maximum scalar dissipation rate is reached at two symmetric points at each side of the bubble, where $\hat{\delta}_{min}^2 \simeq 2.22$. However, the scalar dissipation rate is approximately constant in the forward part of the bubble, its maximum value being only a 4% larger than its value at the forward stagnation point. This confirms that in the planar case the analysis of the centerplane solution is enough to determine the conditions for local flame extinction.

The thickening of the mixing layer in the vicinity of the rear stagnation point is associated with the negative strain imposed by the flow in that region.

2. Axisymmetric case

In the axisymmetric case $\hat{\eta}_{st} = -\alpha_0^{-1/3}(1-\alpha_0^{2/3})^{1/2}$, $\hat{\delta}_{st}^2 = [3\pi\alpha_0^{4/3}(1-\alpha_0^{2/3})^{1/2}]^{-1}$, and the velocity field can be written as

$$\hat{u} = -(2\hat{\xi})^{-3/2}\hat{\eta}I_1(\mu), \tag{52}$$

$$\hat{v} = -(2\hat{\xi})^{-3/2}[I_1(\mu) - \hat{\xi}I_0(\mu)] + \pi\alpha_0, \tag{53}$$

where I_0 and I_1 are given by (24) and (25) with $\mu = (\hat{\xi}^2 + \hat{\eta}^2 + 1)/2\hat{\xi} - 1$. The mixing layer structure obtained from the integration of (48) with the above velocity field is shown in Figs. 8(e) and 8(f), corresponding to $\alpha_0 = 0.5$ and $\alpha_0 = 0.7$, respectively.

The minimum mixing layer thickness, $\hat{\delta}_{min}^2$, along with its quasi-steady value, $\hat{A}_{max}^{-1}$, and the mixing layer thickness at the forward stagnation point, $\hat{\delta}_{st}^2 = \hat{A}_{st}^{-1}$, are shown in Fig. 9 as functions of α_0.

As can be seen, $\hat{\delta}_{min}^2$ decreases monotonically with α_0 whereas $\hat{\delta}_{st}^2$ reaches a minimum for $\alpha_0 = (\frac{4}{5})^{3/2}$, when the strain rate at the forward stagnation point reaches its maximum. Note also that the ratio $\hat{\delta}_{min}^{-2}/\hat{A}_{max}$ of the nondimensional scalar dissipation rate to its quasi-steady value decreases almost linearly from 0.96 for $\alpha_0 = 0.4$ to 0.86 for $\alpha_0 = 1$ due to unsteady effects.

B. Analysis of the second stage of the interaction

The previous analysis can be extended to describe the structure of the mixing layer during the second stage of the interaction by substituting r_0 by r_c as characteristic length scale and $\tilde{\Gamma}$ by $\tilde{\Gamma}_{eff} = \tilde{\Gamma}/(r_c/r_0)^2$ as effective (time-varying)
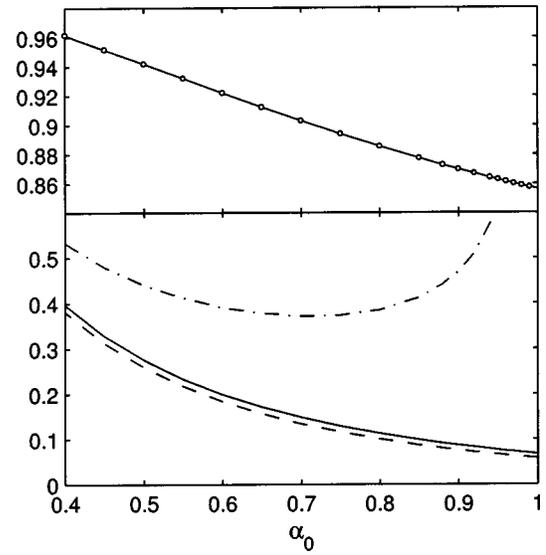

FIG. 9. $\hat{\delta}_{min}^2$ (solid), $\hat{A}_{max}^{-1}$ (dashed), $\hat{\delta}_{st}^2 = \hat{A}_{st}^{-1}$ (dot-dashed), and $\hat{\delta}_{min}^{-2}/\hat{A}_{max}$ (solid-circles) as a function of α_0.

nondimensional vortex strength. The resulting analysis, valid for large values of $\tilde{\Gamma}_{eff}$, gives the evolution of the maximum scalar dissipation rate through Eq. (49) with $\tilde{\Gamma}$ substituted by $\tilde{\Gamma}_{eff}$.

VII. THE INTERACTION OF MIXING LAYERS WITH VORTICES WHEN $\tilde{\Gamma}_{eff} = \tilde{\Gamma}/(r_c/r_0)^2 \ll 1$

When the effective nondimensional vortex strength $\tilde{\Gamma}_{eff} = \tilde{\Gamma}/(r_c/r_0)^2 \sim (l_a/r_c)^2$ is small, the perturbations induced in the vicinity of the vortex core by the second vortex—or by the rest of the vortex ring—are negligible, and in first approximation the problem reduces to the interaction of a single vortex with a counterflow mixing layer. In this case, the characteristic scale l_a of the asymptotic structure of the flow is defined by equating the velocity $\Gamma/2\pi l_a$ induced by the vortex to that due to the strain $A_0 l_a$, which requires $l_a = (\Gamma/2\pi A_0)^{1/2}$.

In the reference frame whose origin moves with the vortex core, the flow field, shown in Fig. 10, becomes stationary, and as the interaction proceeds the mixing layer eventually adopts the form of the dividing streamlines that emerge from the stagnation points $\pm(x_{st}, y_{st})$. This again allows us to evaluate the nondimensional strain rate at the stagnation points $\tilde{A}_{st} = A_{st}/A_0$, and from it the nondimensional thickness of the mixing layer there, $\delta_{st}^2 = \delta_{m,st}^2/\delta_{m0}^2 = \chi_{s0}/\chi_{s,st} = \tilde{A}_{st}^{-1}$.

Here we shall use $x = (r-r_c)/l_a$, $y = (z-z_c)/l_a$, $\bar{u} = (u - dr_c/dt)/A_0 l_a$, $\bar{v} = (v - dz_c/dt)/A_0 l_a$, and $\tau = A_0 t$ as nondimensional variables, with the nondimensional strain rate given by

$$\tilde{A} = \frac{A}{A_0} = \frac{-\bar{v}^2\bar{u}_x + \bar{u}\bar{v}(\bar{v}_x + \bar{u}_y) - \bar{u}^2\bar{v}_y}{\bar{u}^2 + \bar{v}^2}. \tag{54}$$

Then, the integration of the problem

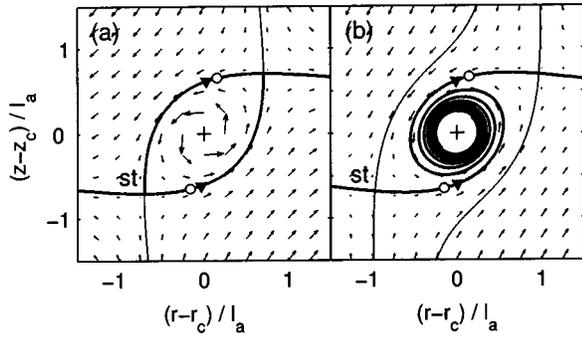FIG. 10. Asymptotic structure of the flow in the vicinity of the vortex core for $\tilde{\Gamma}_{eff} = \tilde{\Gamma}/(r_c/r_0)^2 \ll 1$, showing the dividing streamlines that emerge from the stagnation points (st) and the asymptotic position of the mixing layer for large times (thick solid lines): (a) two-dimensional case; (b) axisymmetric case. The points of maximum strain (hollow circles) and maximum scalar dissipation rate (solid triangles) are clearly indicated.

$$\frac{d}{d\tau}\left\{\begin{array}{c} x \\ y \\ \delta^2 \end{array}\right\} = \left\{\begin{array}{c} \bar{u} \\ \bar{v} \\ 2 - 2\tilde{A}\delta^2 \end{array}\right\}, \tag{55}$$

with the initial condition $\delta^2 = \delta_{st}^2$ imposed close to the stagnation points, provides the spatial evolution of the scalar dissipation rate along the dividing streamline.

Notice that when $\tilde{\Gamma} \ll 1$ the effective nondimensional vortex strength $\tilde{\Gamma}_{eff} = \tilde{\Gamma}/(r_c/r_0)^2$ is already small when the vortices cross the original plane of the mixing layer, so that the previous analysis will hold during all the interaction. On the other hand, for $\tilde{\Gamma} \gtrsim 1$ one should wait times of order $A_0^{-1} \log \tilde{\Gamma}$ after the beginning of the interaction to reach small values of $\tilde{\Gamma}_{eff}$. In this case the previous analysis will only hold at times such that the radius of the vortex is large compared to $r_0 \tilde{\Gamma}^{1/2}$.

A. Two-dimensional case

In the two-dimensional case, the asymptotic velocity field in the reference frame moving with the vortex core is

$$\bar{u} = x - \frac{y}{x^2+y^2}, \quad \bar{v} = -y + \frac{x}{x^2+y^2}, \tag{56}$$

corresponding to the superposition of a two-dimensional stagnation flow with velocity gradients 1 and -1 along the x and y axis, and a point vortex of unit strength located at the origin. In this case, the strain rate at the stagnation points, $x_{st} = y_{st} = 2^{-1/2}$, is given by $\delta_{st}^{-2} = \tilde{A}_{st} = 2$.

When measured with its unperturbed value, the maximum scalar dissipation rate obtained by integrating (55) with the above velocity field is $\chi_{s,max}/\chi_{s0} = \delta_{min}^{-2} \simeq 2.57$, a value that does not depend on the strength of the vortices. This explains the apparently paradoxical result, observed in Fig. 6, that the peak scalar dissipation rate tends to a constant value for large times regardless of the strength of the vortices.

The location of the points of maximum strain and of maximum scalar dissipation rate is also shown in Fig. 10.

B. Axisymmetric case

In the axisymmetric case, the asymptotic velocity field in the reference frame moving with the vortex core is

$$\bar{u} = \frac{x}{2} - \frac{y}{x^2+y^2}, \quad \bar{v} = -y + \frac{x}{x^2+y^2}, \quad \bar{w} = \frac{\zeta}{2}, \tag{57}$$

where ζ represents the local azimuthal coordinate and $\bar{w}$ the corresponding velocity component, measured with l_a and $A_0 l_a$, respectively.

The above velocity field corresponds to the superposition of a three-dimensional stagnation point flow, with velocity gradients $\frac{1}{2}$ along the x and ζ axes and -1 along the y axis, and a line vortex of unit strength located along the ζ axis. In the axisymmetric case the azimuthal strain associated with the growing radius of the vortex ring induces an average negative radial velocity towards the core. As shown in Fig. 10(b), this forces the streamlines to spiral into the origin, resulting in a continuous ingestion of fluid towards the core. This is in contrast to the closed streamlines obtained in the two-dimensional case shown in Fig. 10(a).

At the stagnation points, where $x_{st} = 2^{3/4}3^{-1/2}$, $y_{st} = 2^{1/4}3^{-1/2}$, we have $\delta_{st}^{-2} = \tilde{A}_{st} \simeq 1.69$. In this case the integration of (55) with the velocity field given in (57) gives $\chi_{s,max}/\chi_{s0} = \delta_{min}^{-2} \simeq 2.54$. This value is surprisingly close to the two-dimensional value and is also plotted in Fig. 6.

VIII. CONCLUSIONS

A constant density model has been presented for the low Mach number interaction of vortex pairs and vortex rings with counterflow reacting mixing layers in the limiting case when the characteristic thickness of the mixing layer is small compared to the characteristic size of the vortices. This simplified approach presents many advantages, like introducing analytical solutions for the velocity field. This leads to analytic developments that reduce the problem to solve a system of ordinary differential equations. In particular, the structure of the mixing layer is investigated using the classical mixture fraction variable Z and neglecting curvature effects. This permits us to find a self-similar solution, which allows us to identify some of the key physical mechanisms involved in flame–vortex interactions.

For large values of the nondimensional vortex strength the interaction can be split in three different stages, which can be described asymptotically in good agreement with the numerical results. The first stage determines the conditions for local flame extinction, the second stage determines the conditions for pocket formation and triple flame propagation, and the third stage reduces to the interaction of a single vortex with a strained mixing layer.

In the planar case the scalar dissipation rate is almost constant and very close to its maximum value up to distances of order r_c from the center plane. The center plane solution can then be used to predict the conditions of local flame extinction. On the other hand, in the axisymmetric case the maximum scalar dissipation rate turns out to be much higher than its value at the symmetry axis, and a detailed analysis of the dynamics of the whole mixing layer is needed. In this

Phys. Fluids, Vol. 16, No. 7, July 2004

On the interaction of vortices with mixing layers   2251

case the maximum scalar disipation rate is reached in an annular region at radial distances of order r_c away from the origin, leading in some cases to the existence of an annular extinction regime similar to that observed by Katta *et al.*[30]

For small values of the nondimensional vortex strength the interaction takes place as if the vortices were isolated, and the analysis reduces again to the interaction of a single vortex with a strained mixing layer.

It is important to note that, as can be demonstrated by simple kinematical arguments, the results presented herein remain valid even when the symmetry axis of the vortices does not coincide with that of the basic flow, as long as both axes are parallel and the vortices propagate normal to the unperturbed mixing layer. In this case we only need to choose a reference frame with origin at the midpoint between the vortex cores, or at the center of the vortex ring, to reduce the problem to that analyzed here.

The assumption that the density is constant throughout the mixing layer, which allowed us to write Eq. (36), can be relaxed without difficulty in the near-axis region, where a similarity transformation can be used to simplify the governing equations to a set of one-dimensional equations even if density changes are fully taken into account. This more realistic case presents overshoots in the tangential velocity u_s due to the stronger accelerations suffered by the hot combustion gases in the mixing layer, which in turn modify the velocity component u_n normal to the mixing layer, that will no longer be given by Eq. (33). Then, the strain rate A varies across the mixing layer so that Eq. (35) no longer applies to yield a closed form description of Z. Far from the axis the problem does not admit any simplifications and the solution has to be obtained numerically.

Despite the apparent simplicity of the analysis, it has led to results that are in qualitative agreement with the experimental results of Santoro *et al.*[32–35] In particular, Santoro[35] claims that, during the interaction of the diffusion flame with a strong vortex, the constant density model reproduces qualitatively well the experimental evolution of the strain rate, A, and the scalar dissipation rate, χ_s, at the axis of symmetry as long as A and χ_s are nondimensionalized with their baseline strain values. This is in agreement with recent numerical simulations carried out in our group concerning the effects of dilatation on the structure of unsteady mixing layers.

The analysis has also contributed to the understanding of previously unclear phenomena, such as the annular extinction regime first observed by Katta *et al.*[30] However, it should be kept in mind that this work constitutes only a first step towards the understanding, using asymptotic techniques, of the complex physical mechanisms involved in flame vortex interaction.

ACKNOWLEDGMENTS

APPENDIX: THE SELF-INDUCED VELOCITY OF A VORTEX RING SUBJECT TO STRAIN

In this appendix we analyze the vorticity distribution of a vortex ring of circulation Γ subject to a coaxial, axisymmetric strain with axial and radial velocity gradients $-A_0$ and $A_0/2$, respectively.

It is well known that the dynamics of a vortex ring of radius r_c and circulation Γ depends on the characteristic size δ_v of the vorticity core.[42] Since the circulation of the strained vortex ring is constant and the vortex ring radius is completely determined by the underlying strain, we only need to calculate the time evolution of the vortex core thickness δ_v to completely determine the dynamics of the vortex ring.

Thus, let us define the vortex core size as

$$\delta_v^2 = \frac{2\pi}{\Gamma} \int_0^\infty r^3 \omega(\rho, t) dr. \tag{A1}$$

Then, the ratio of the characteristic viscous time, δ_v^2/ν, to the characteristic strain time, A_0^{-1}, defines the Reynolds number of the vortex core

$$\text{Re}_v = \frac{\delta_v^2 A_0}{\nu}, \tag{A2}$$

which can also be viewed as the square of the nondimensional vortex core size based on the characteristic viscous length $(\nu/A_0)^{1/2}$.

For small Reynolds numbers the dynamics of the vortex core will be dominated by viscosity, while for large Reynolds numbers it will be essentially inviscid. However, in both cases the size of the vortex core will tend to a constant value of the order of $(\nu/A_0)^{1/2}$ as a result of the radial competition between convection and diffusion.

In what follows, we consider a reference frame (x, y, ζ) moving with the vortex core, where x and y are the radial and axial coordinates, and ζ represents the local azimutal coordinate. As discussed in Sec. VII B, in this reference frame the asymptotic velocity field at small distances from the vortex core corresponds, in first approximation, to the superposition of a three-dimensional stagnation point flow with velocity gradients $A_0/2$ along the x and ζ axes and $-A_0$ along the y axis, and a line vortex of strength Γ located along the ζ axis.

In reality, however, the vorticity will be distributed over a region of characteristic size δ_v around the ζ axis. In the present analysis we shall assume that the characteristic size of the vorticity distribution is small compared with the characteristic scale $(\Gamma/A_0)^{1/2}$ of the asymptotic structure of the flow. Then, the vorticity is confined to a small core around the origin, with

$$\text{Re}_\Gamma = \frac{\omega_c}{A_0} \text{Re}_v \gg \text{Re}_v, \tag{A3}$$

where $\text{Re}_\Gamma = \Gamma/\nu$ is the Reynolds number based on the vortex circulation, assumed here to be much larger than one, and $\omega_c = \Gamma/\delta_v^2$ is the characteristic value of the vorticity in the

core. As a consequence, the characteristic turnover time ω_c^{-1} will be small compared with the characteristic strain time A_0^{-1}.

Thus we will seek a solution of the vorticity equation

$$\frac{\partial \omega}{\partial t} + \mathbf{u} \cdot \nabla \omega = \omega \cdot \nabla \mathbf{u} + \nu \nabla^2 \omega, \tag{A4}$$

in which there is only a ζ component of vorticity, assuming that both the vorticity and the velocity induced by it are independent of ζ. Introducing cylindrical-polar coordinates (ρ, θ, ζ), with $x = \rho \cos \theta$ and $y = \rho \sin \theta$, we may write

$$u_\zeta = \frac{A_0}{2} \zeta, \tag{A5a}$$

$$u_\rho = \left(-\frac{1}{2} + \frac{3}{2} \cos 2\theta \right) \frac{A_0}{2} \rho + u_\rho'(\rho, \theta, t), \tag{A5b}$$

$$u_\theta = \left(-\frac{3}{2} \sin 2\theta \right) \frac{A_0}{2} \rho + u_\theta'(\rho, \theta, t), \tag{A5c}$$

where u_ρ' and u_θ' represent the perturbation velocity field induced by the vorticity distribution

$$\omega(\rho, \theta, t) = \frac{1}{\rho} \frac{\partial(\rho u_\theta')}{\partial \rho} - \frac{1}{\rho} \frac{\partial u_\rho'}{\partial \theta}. \tag{A6}$$

Then, Eq. (A4) can be written as

$$\frac{\partial \omega}{\partial t} + \left[\left(-\frac{1}{2} + \frac{3}{2} \cos 2\theta \right) \frac{A_0}{2} \rho + u_\rho' \right] \frac{\partial w}{\partial \rho}$$

$$+ \left[\left(-\frac{3}{2} \sin 2\theta \right) \frac{A_0}{2} + \frac{u_\theta'}{\rho} \right] \frac{\partial \omega}{\partial \theta}$$

$$= \frac{A_0}{2} \omega + \nu \left[\frac{1}{\rho} \frac{\partial}{\partial \rho} \left(\rho \frac{\partial \omega}{\partial \rho} \right) + \frac{1}{\rho^2} \frac{\partial^2 \omega}{\partial \theta^2} \right] \tag{A7}$$

to be integrated with the boundary condition $\omega \to 0$ at $\rho \to \infty$, and regularity conditions at $\rho = 0$, while the continuity equation for the perturbation velocity field, u_ρ' and u_θ', adopts the two-dimensional form

$$\frac{\partial r u_\rho'}{\partial \rho} + \frac{\partial u_\theta'}{\partial \theta} = 0, \tag{A8}$$

so that a stream function ψ may be introduced, such that $\omega = -\nabla^2 \psi$, with $u_\rho' = (1/\rho) \partial \psi / \partial \theta$, $u_\theta' = -\partial \psi / \partial \rho$.

Introducing $(\nu/A_0)^{1/2}$, A_0, $\Gamma/(\nu/A_0)^{1/2}$, and $A_0 \Gamma / \nu$ as length, time, velocity and vorticity scales, respectively, Eq. (A7) takes the nondimensional form

$$u_\rho' \frac{\partial w}{\partial \rho} + \frac{u_\theta'}{\rho} \frac{\partial w}{\partial \theta} + \frac{1}{\text{Re}_\Gamma} \left[\frac{\partial \omega}{\partial \tau} + \left(-\frac{1}{2} + \frac{3}{2} \cos 2\theta \right) \frac{\rho}{2} \frac{\partial w}{\partial \rho} \right.$$

$$\left. + \left(-\frac{3}{2} \sin 2\theta \right) \frac{1}{2} \frac{\partial \omega}{\partial \theta} \right]$$

$$= \frac{1}{\text{Re}_\Gamma} \left[\frac{w}{2} + \frac{1}{\rho} \frac{\partial}{\partial \rho} \left(\rho \frac{\partial \omega}{\partial \rho} \right) + \frac{1}{\rho^2} \frac{\partial^2 \omega}{\partial \theta^2} \right], \tag{A9}$$

where $\tau = A_0 t$ is the nondimensional time based on A_0^{-1} and for the rest of the variables we maintain the notation used in the dimensional formulation.

In the limit $\text{Re}_\Gamma \to \infty$, the vorticity is strongly localized at the origin, and (A9) is identically satisfied by any axisymmetric distribution of vorticity, for which both u_ρ' and $\partial \omega / \partial \theta$ are identically zero. In this limit, when $u_\theta' = \Gamma/(2\pi\rho)$, the velocity field (A5) corresponds to the superposition of a three-dimensional stagnation point flow with velocity gradients $A_0/2$ along the x and ζ axis and $-A_0$ along the y axis, and a line vortex of strength Γ located along the ζ axis.

For $\text{Re}_\Gamma \gg 1$, the vorticity distribution is slightly non-axisymmetric, and the radial velocity u_ρ' and the azimuthal derivative $\partial \omega / \partial \theta$ are both of order Re_Γ^{-1}. Moreover, the continuity equation provides the estimate $\partial u_\theta' / \partial \theta \sim u_\rho'$, which suggests expanding the solution in powers of Re_Γ^{-1} as

$$\omega(\rho, \theta, t) = \omega_0(\rho, t) + \text{Re}_\Gamma^{-1} \omega_1(\rho, \theta, t) + \cdots, \tag{A10a}$$

$$u_\rho'(\rho, \theta, t) = \text{Re}_\Gamma^{-1} u_{\rho 1}'(\rho, \theta, t) + \cdots, \tag{A10b}$$

$$u_\theta'(\rho, \theta, t) = u_{\theta 0}'(\rho, t) + \text{Re}_\Gamma^{-1} u_{\theta 1}'(\rho, t) + \cdots. \tag{A10c}$$

Introducing this expansion in Eq. (A9) and integrating from $\theta = 0$ to 2π, we obtain the following equation for the leading order vorticity distribution:

$$\frac{\partial \omega_0}{\partial \tau} - \frac{\rho}{4} \frac{\partial \omega_0}{\partial \rho} = \frac{\omega_0}{2} + \frac{1}{\rho} \frac{\partial}{\partial \rho} \left(\rho \frac{\partial \omega_0}{\partial \rho} \right). \tag{A11}$$

As shown by Lundgren,[56] solutions to this equation may be found from solutions of strictly two-dimensional flows with the same initial conditions by means of the transformation

$$\omega_0(\rho, \tau) = e^{\tau/2} \Omega \left(e^{\tau/4} \rho, \frac{e^{\tau/2} - 1}{1/2} \right), \tag{A12}$$

where the function $\Omega(\rho', \tau')$ satisfies the axisymmetric heat equation

$$\frac{\partial \Omega}{\partial \tau'} = \frac{1}{\rho'} \frac{\partial}{\partial \rho'} \left(\rho' \frac{\partial \Omega}{\partial \rho'} \right). \tag{A13}$$

However, it is well known that any axisymmetric vortex will decay to Gaussian with time.[57] Thus, in what follows we shall restrict our attention to solutions of the form

$$\Omega(\rho', \tau') = \frac{1}{\pi \delta_\Omega^2} \exp \left(-\frac{\rho'^2}{\delta_\Omega^2} \right), \tag{A14}$$

where the vorticity Ω has been scaled in order to adjust the circulation of the vortex to its unitary nondimensional value $\int_0^\infty 2\pi \rho' \Omega(\rho', \tau') d\rho' = 1$.

Substituting (A14) into (A13) we obtain $d\delta_\Omega^2 / d\tau' = 4$, which can be integrated with the initial condition $\delta_\Omega^2(0) = \delta_0^2$ to give $\delta_\Omega^2 = \delta_0^2 + 4\tau'$. Then, Eq. (A14) implies that the amplitude of the vorticity distribution should decrease inversely with time, which guarantees that the vortex circulation is constant.

According to Lundgren's transformation, the leading order vorticity distribution ω_0 will be given by

Phys. Fluids, Vol. 16, No. 7, July 2004

On the interaction of vortices with mixing layers   2253

$$\omega_0(\rho, \tau) = \frac{1}{\pi} \frac{1}{\mathrm{Re}_v} \exp\left(-\frac{\rho^2}{\mathrm{Re}_v}\right), \qquad (A15)$$

with Re_v given by

$$\mathrm{Re}_v = 8 + (\mathrm{Re}_{v0} - 8)e^{-\tau/2} \qquad (A16)$$

in terms of its value $\mathrm{Re}_{v0} = \delta_{v0}^2 A_0/\nu$ at $\tau=0$. Note that for $\mathrm{Re}_{v0} < 8$ this equation predicts a vortex core radius which shrinks to zero for $\tau = \tau^* = 2\log(1 - \mathrm{Re}_{v0}/8) < 0$.

The previous analysis shows that for large values of the Reynolds number Re_Γ, an approximately Gaussian and sufficiently compact vortex will maintain its shape during its evolution, decreasing or increasing its size depending on the initial value of Re_v as a result of the radial competition between convection and diffusion. In both cases, the nondimensional vortex core size will tend to the constant value $\delta_v/(\nu/A_0)^{1/2} = \mathrm{Re}_v^{1/2} = 8^{1/2}$.

Once the time evolution of the core size is known, the self-induced velocity of the vortex ring is given by the expression

$$V_I = \frac{\Gamma}{4\pi r_c}\left(\log\frac{8r_c}{\delta_v} - 0.558\right), \qquad (A17)$$

derived by Saffman[58] for vortices with a Gaussian vorticity core, such as (A15).

[1] F. A. Williams, *Combustion Theory*, 2nd ed. (Benjamin/Cummings, Menlo Park, CA, 1985).

[2] P. H. Renard, D. Thévenin, J. C. Rolon, and S. Candel, "Dynamics of flame/vortex interactions," Prog. Energy Combust. Sci. **26**, 225 (2000).

[3] N. Peters, *Turbulent Combustion* (Cambridge University Press, Cambridge, 2000).

[4] A. Liñán, "The asymptotic analysis of counterflow diffusion flames for large activation energies," Acta Inf. **1**, 1007 (1974).

[5] B. Cuenot, F. N. Egolfopoulos, and T. Poinsot, "An unsteady laminar flamelet model for non-premixed combustion," Combust. Theory Modell. **4**, 77 (2000).

[6] N. Peters, "Laminar flamelet concepts in turbulent combustion," Proc. Combust. Inst. **21**, 1231 (1986).

[7] B. Cuenot and T. Poinsot, "Effects of curvature and unsteadiness in diffusion flames. Implications for turbulent diffusion combustion," Proc. Combust. Inst. **25**, 1383 (1994).

[8] D. C. Haworth, M. C. Drake, S. B. Pope, and R. J. Blint, "The importance of time-dependent flame structures in stretched laminar flamelet models for turbulent jet diffusion flames," Proc. Combust. Inst. **22**, 589 (1988).

[9] H. Pitsch, M. Chan, and N. Peters, "Unsteady flamelet modeling of turbulent hydrogen–air diffusion flames," Proc. Combust. Inst. **27**, 1057 (1998).

[10] T. Saitoh and Y. Otsuka, "Unsteady behavior of diffusion flames and premixed flames for counterflow geometry," Combust. Sci. Technol. **12**, 135 (1976).

[11] N. Darabiha, "Transient behavior of laminar counterflow hydrogen–air diffusion flames with complex chemistry," Combust. Sci. Technol. **86**, 163 (1992).

[12] A. F. Ghoniem, M. C. Soteriou, and O. M. Knio, "Effect of steady and periodic strain on unsteady flamelet combustion," Proc. Combust. Inst. **24**, 223 (1992).

[13] R. S. Barlow and J. Y. Chen, "On transient flamelets and their relationship to turbulent methane–air jet flames," Proc. Combust. Inst. **24**, 231 (1992).

[14] F. N. Egolfopoulos and C. S. Cambell, "Unsteady counterflowing strained diffusion flames: Diffusion-limited frequency response," J. Fluid Mech. **318**, 1 (1996).

[15] H. Pitsch and S. Fedotov, "Investigation of scalar dissipation rate fluctuations in non-premixed turbulent combustion using a stochastic approach," Combust. Theory Modell. **5**, 41 (2001).

[16] F. E. Marble, "Growth of a diffusion flame in the field of a vortex," in *Recent Advances in the Aerospace Science*, edited by C. Casci (Plenum, New York, 1985), p. 395.

[17] A. R. Karagozian and F. E. Marble, "Study of a diffusion flame in a stretched vortex," Combust. Sci. Technol. **45**, 65 (1986).

[18] H. R. Baum, D. M. Corley, and R. G. Rehm, "Time-dependent simulation of small scale turbulent mixing and reaction," Proc. Combust. Inst. **21**, 1263 (1986).

[19] B. M. Cetegen and W. A. Sirignano, "Study of mixing and reaction in the field of a vortex," Combust. Sci. Technol. **72**, 157 (1990).

[20] A. Liñán, *El papel de la mecánica de fluidos en los procesos de combustión* (Real Academia de Ciencias Exactas, Físicas y Naturales, Madrid, 1991).

[21] N. Peters and F. A. Williams, "Premixed combustion in a vortex," Proc. Combust. Inst. **22**, 495 (1988).

[22] A. R. Karagozian and B. V. S. Manda, "Flame structure and fuel consumption in the field of a vortex pair," Combust. Sci. Technol. **49**, 185 (1986).

[23] A. Laverdant and S. Candel, "Computation of diffusion and premixed flames rolled up in vortex structures," J. Propul. Power **5**, 134 (1989).

[24] D. Thévenin and S. Candel, "Ignition dynamics of a diffusion flame rolled up in a vortex," Phys. Fluids **7**, 434 (1995).

[25] F. Takahashi and V. R. Katta, "Numerical experiments on the flame–vortex interactions in a jet diffusion flame," J. Propul. Power **11**, 170 (1995).

[26] T. Poinsot, A. Trouvé, D. Veynante, S. Candel, and E. Esposito, "Vortex driven acoustically coupled combustion instabilities," J. Fluid Mech. **177**, 265 (1987).

[27] C. J. Mueller and R. W. Schefer, "Coupling of diffusion flame structure to an unsteady vortical flowfield," Proc. Combust. Inst. **27**, 1105 (1998).

[28] Y. H. You, D. K. Lee, and H. D. Shin, "Visual investigation of a vortex ring interacting with a nonpremixed flame," Combust. Sci. Technol. **139**, 365 (1998).

[29] W. L. Roberts, J. F. Driscoll, M. C. Drake, and J. W. Ratcliffe, "OH fluorescence images of the quenching of a premixed flame during an interaction with a vortex," Proc. Combust. Inst. **24**, 169 (1992).

[30] V. R. Katta, C. D. Carter, G. J. Fiechtner, W. M. Roquemore, J. R. Gord, and J. C. Rolon, "Interaction of a vortex with a flat flame formed between opposing jets of hydrogen and air," Proc. Combust. Inst. **27**, 587 (1998).

[31] P. H. Renard, J. C. Rolon, D. Thévenin, and S. Candel, "Investigations of heat release, extinction, and time evolution of the flame surface, for a nonpremixed flame interacting with a vortex," Combust. Flame **117**, 189 (1999).

[32] V. S. Santoro, D. C. Kyritsis, and A. Gómez, "Extinction behaviour of either gaseous or spray counterflow diffusion flames interacting with a laminar toroidal vortex," in *Seventeenth International Colloquium on the Dynamics of Explosions and Reactive Systems* (1999).

[33] V. S. Santoro, D. C. Kyritsis, A. Liñán, and A. Gómez, "Vortex-induced extinction behavior in methanol gaseous flames: A comparison with quasi-steady extinction," Proc. Combust. Inst. **28**, 2109 (2000).

[34] V. S. Santoro, A. Liñán, and A. Gómez, "Propagation of edge flames in counterflow mixing layers: Experiments and theory," Proc. Combust. Inst. **28**, 2039 (2000).

[35] V. S. Santoro, "The interaction of laminar vortices with diffusion flames," Ph.D. thesis, Yale University, 2002.

[36] C. Safta, S. Enachescu, and C. K. Madnia, "Interaction of a vortex ring with a diffusion flame," Phys. Fluids **14**, 668 (2002).

[37] D. Thévenin, P.-H. Renard, J. C. Rolon, D. W. Kendrick, D. Veynante, and S. Candel, "Structure of a non-premixed flame interacting with counter-rotating vortices," Proc. Combust. Inst. **26**, 1079 (1996).

[38] F. E. Marble and J. E. Broadwell, "The coherent flame model of non-premixed turbulent combustion," Project Squid Report TRW-9-PU (1977).

[39] J. W. Dold, "Flame propagation in a nonuniform mixture: Analysis of a slowly varying triple flame," Combust. Flame **76**, 71 (1989).

[40] J. Daou and A. Liñán, "The role of unequal diffusivities in ignition and extinction fronts in strained mixing layers," Combust. Theory Modell. **2**, 449 (1998).

[41] Lord Kelvin, "The translatory velocity of a circular vortex ring," Philos. Mag. **37(4)**, 511 (1867).

[42] G. Saffman, *Vortex Dynamics* (Cambridge University Press, Cambridge, 1992).

[43] W. J. A. Dahm, C. M. Scheil, and G. Tryggvason, "Dynamics of vortex interaction with a density interface," J. Fluid Mech. **205**, 1 (1989).

[44] D. L. Marcus and J. B. Bell, "Numerical simulation of a viscous vortex ring interaction with a density interface," Phys. Fluids **6**, 1505 (1994).

[45]T. Miloh and D. J. Shlien, "Passage of a vortex ring through a circular aperture in an infinite plane," Phys. Fluids **20**, 1219 (1977).

[46]T. Miyazaki and T. Kambe, "Axisymmetric problem of vortex sound with solid surfaces," Phys. Fluids **29**, 4006 (1986).

[47]P. A. Tyvand and T. Miloh, "Axysimmetric interaction between a vortex ring and a free surface," Phys. Fluids **6**, 224 (1994).

[48]K. Shariff, A. Leonard, and J. H. Ferziger, "Dynamics of a class of vortex rings," NASA Technical Memorandum 102257 (1989).

[49]G. F. Carrier, F. E. Fendell, and F. E. Marble, "The effect of strain rate on diffusion flames," SIAM (Soc. Ind. Appl. Math.) J. Appl. Math. **28**, 463 (1975).

[50]A. Liñán and F. A. Williams, "Ignition in an unsteady mixing layer subject to strain and variable pressure," Combust. Flame **95**, 31 (1993).

[51]J. R. Cash and A. H. Karp, "A variable order Runge–Kutta method for initial value problems with rapidly varying right-hand sides," ACM Trans. Math. Softw. **16**, 201 (1990).

[52]W. H. Press, S. A. Teukolsky, W. T. Vetterling, and B. P. Flannery, *Numerical Recipes in Fortran 77: The Art of Scientific Computing*, 2nd ed. (Cambridge University Press, Cambridge, 1992).

[53]J. Daou, "Ignition and combustion of fuel pockets moving in an oxidizing atmosphere," Combust. Flame **115**, 383 (1998).

[54]S. E. Widnall and C.-Y. Tsai, "The instability of the thin vortex ring of constant vorticity," Proc. R. Soc. London **287**, 273 (1977).

[55]P. G. Saffman, "The number of waves on unstable vortex rings," J. Fluid Mech. **84**, 625 (1978).

[56]T. S. Lundgren, "Strained spiral vortex model for turbulent fine structure," Phys. Fluids **25**, 2193 (1982).

[57]J. Jimenez, "Hyperviscous vortices," J. Fluid Mech. **279**, 169 (1994).

[58]P. G. Saffman, "The velocity of viscous vortex rings," Stud. Appl. Math. **49**, 371 (1970).